New chlorophylls designed by theoretical spectroscopy and machine learning

Fabian Weber,[a] Simon Petry,[a] Dennis Nürnberg[b,c] and Jan P. Götze[a,*]

[a]*Freie Universität Berlin, Fachbereich Biologie Chemie Pharmazie, Physikalische und Theoretische Chemie, Arnimallee 22, 14195 Berlin, Germany*

[b]*Freie Universität Berlin, Fachbereich Physik, Experimentelle Biophysik, Arnimallee 14, 14195 Berlin, Germany*

[c]*Freie Universität Berlin, Dahlem Centre of Plant Sciences, Albrecht-Thaer-Weg 6, 14195 Berlin, Germany*

Corresponding author, email: jan.goetze@fu-berlin.de

Supporting information

Table of contents

S1: Core structure used in this study

Below, the core structure of the all-hydrogen substituted chlorophyll is given in xyz-format. Comments given at the side (i.e. ! x1) are relevant for the ArchOnML package.

```
      57

C     2.234005   -0.357089  -0.315353
C     -1.349956  -1.465035  -0.250820
C     -1.997212  -2.721898  -0.311001
C     -3.432475  -2.505858  -0.427705
C     -3.642984  -0.943202  -0.378785
C     -1.009123  -3.695588  -0.265646  !X3
C     0.226336   -2.955004  -0.177569
N     -0.033190  -1.589971  -0.170385
C     1.525058   -3.461812  -0.126212
C     2.711368   -2.722234  -0.081215
C     4.046428   -3.275111  -0.019263  !X2
C     4.911257   -2.204794  0.000658   !X1
C     4.090433   -1.018416  -0.056902
N     2.781756   -1.349407  -0.102713
C     4.582791   0.312590   -0.067226
C     3.854923   1.480119   -0.129933
C     4.409427   2.834223   -0.137054  !X6
C     3.345891   3.695628   -0.210968  !X5
C     2.144590   2.866634   -0.232626
N     2.480369   1.560415   -0.182628
C     0.832243   3.363234   -0.297188
C     -0.358889  2.647309   -0.326015
N     -0.491129  1.307700   -0.286080
C     -1.822403  0.950376   -0.343289
C     -2.703133  2.174195   -0.508125
C     -1.709760  3.343299   -0.372634  !X4
Mg    1.202054   -0.006661  -0.189726
H     -1.851991  4.394341   -1.469398  !Y4
C     -3.918742  2.255200   0.419834
C     -3.605422  2.097020   1.906295
C     -4.807309  1.672525   2.708410
O     -5.676548  0.935403   2.315711
H     3.354039   5.185768   -0.301558  !Y5
H     5.841000   3.131376   -0.101509  !Y6
H     4.387777   -4.733148  0.061594   !Y2
H     -1.175873  -5.177883  -0.311561  !Y3
O     -4.328972  -3.309711  -0.533100
C     -4.452885  -0.455022  -1.579909
O     -3.926413  0.011834   -2.553671
O     -5.782341  -0.529983  -1.523350
C     -6.499148  -1.057085  -0.408281
O     -4.803838  2.167784   3.949336
H     6.405496   -2.219602  0.068885   !Y1
H     5.666915   0.417194   -0.015978
H     0.733408   4.448033   -0.321626
H     1.626487   -4.548932  -0.127331
```

H	-5.583138	1.805889	4.403665
H	-3.176030	3.002191	2.355978
H	-4.422827	3.220559	0.249299
H	-4.207390	-0.741871	0.545717
H	-7.552826	-1.059457	-0.712413
H	-6.177466	-2.082907	-0.191203
H	-6.383258	-0.414093	0.476854
H	-1.850652	3.841875	0.602892
H	-3.087311	2.141354	-1.541419
H	-4.656259	1.494165	0.137686
H	-2.860455	1.294262	2.050497

S2: Training settings of ArchOnML

For determining the hyperparameters of the Kernel Ridge Regression (KRR) models, a grid-based scan is performed in a 5-fold cross-validation. To define the scanned grid regions, four parameters called `MinMod`, `MaxMod`, `Lambda_Bot` and `Lambda_Top` have to be given by the user. The first two determine how ArchOnML's dynamic grid set-up procedure modifies the σ region, and the latter two give the lowest and highest values of the λ grid in exponential (10^N) fashion. These parameters are currently determined on a trial-and-error basis for each trained property, using sparse grid resolutions at first, and then increasing grid resolution for the actual scan. For all models, the final resolution was chosen to be 32 × 32 grid-points. Below, the settings for all properties will be listed.

- $\Delta E(Q_1)$: `MinMod = 0.00001, MaxMod = 100, Lambda_Bot = -6, Lambda_Top = 1`
- $f(Q_1)$: `MinMod = 0.01, MaxMod = 50, Lambda_Bot = -4, Lambda_Top = 1`
- $\Delta E(Q_2)$: `MinMod = 0.001, MaxMod = 50, Lambda_Bot = -6, Lambda_Top = 1`
- $f(Q_2)$: `MinMod = 1, MaxMod = 100, Lambda_Bot = -6, Lambda_Top = -1`
- $\Delta E(B_1)$: `MinMod = 1, MaxMod = 100, Lambda_Bot = -7, Lambda_Top = -3`
- $f(B_1)$: `MinMod = 0.001, MaxMod = 20, Lambda_Bot = -5, Lambda_Top = 1`
- $\Delta E(B_2)$: `MinMod = 0.1, MaxMod = 100, Lambda_Bot = -5, Lambda_Top = -1`
- $f(B_2)$: `MinMod = 0.01, MaxMod = 20, Lambda_Bot = -5, Lambda_Top = 1`
- $E(T_1)$: `MinMod = 0.00001, MaxMod = 100, Lambda_Bot = -6, Lambda_Top = 1`

Q_1 was always assigned to be the S_1/Q_y state, and Q_2 to be S_2/Q_x. The assignment of the B states was more involved, see sec. S6 below.

S3: Learning curves for all models

On the following pages, the learning curves for all nine trained properties will be presented. As described in the main text, five individual learning curves were generated for each property to check the robustness of each model. Robustness means that for a different random training-testing-split, the overall performance does not change. Note that splitting off the test data was performed before stratification during training. This way, a completely random set of unknown molecules is used for checking performances, which reflects a more realistic situation.

The five individual curves will show both training and testing results for the coefficient of determination r^2 as well as the mean absolute error (MAE) at different amounts of training data during cross-validation. After these, the mean curves for r^2 are given, displaying both the best and worst individual results at each percentage – as well as the mean of all five curves for the training and testing, respectively.

S3a: Learning curves for $\Delta E(Q_1)$

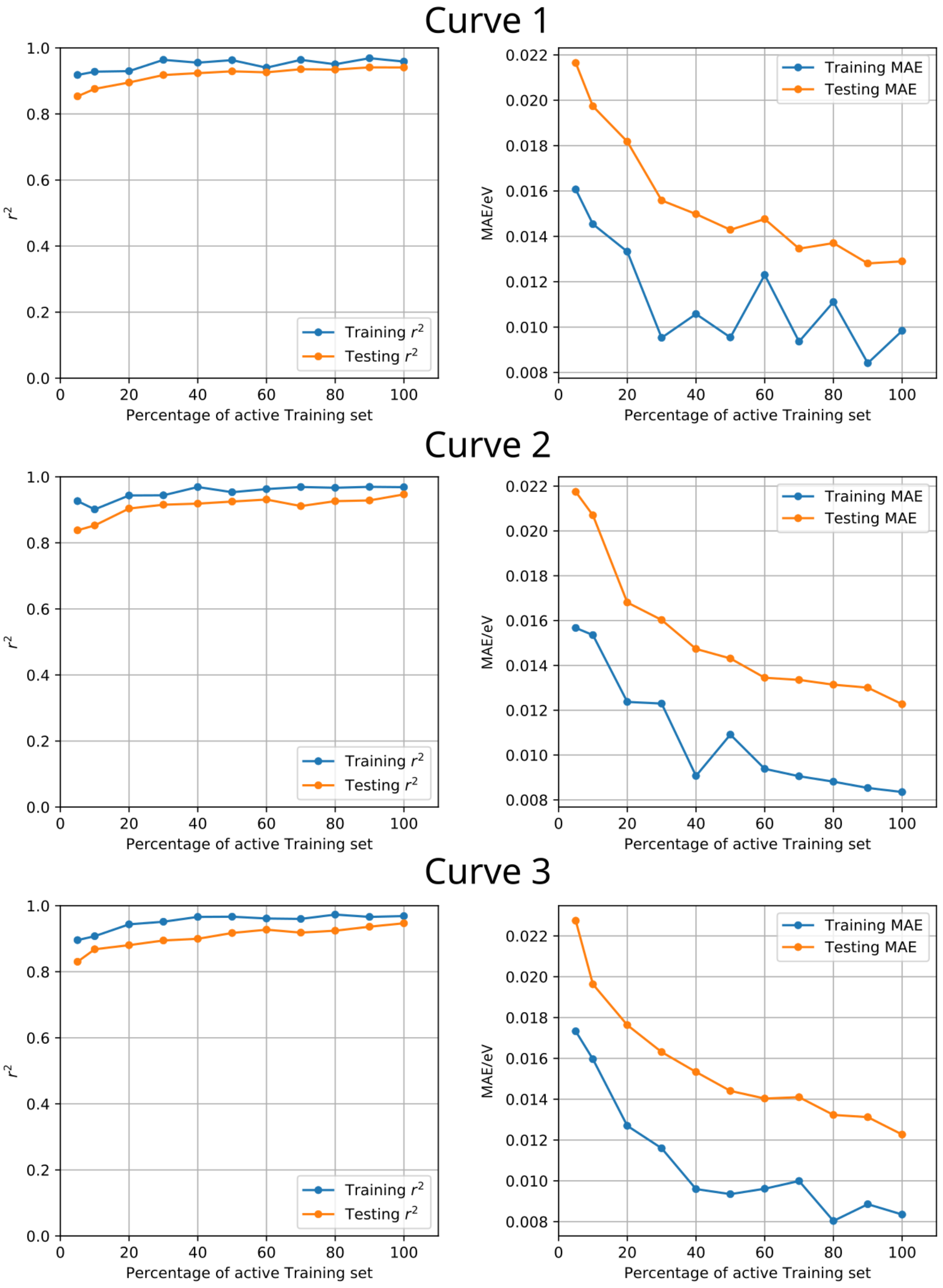
Curve 1

Curve 2

Curve 3

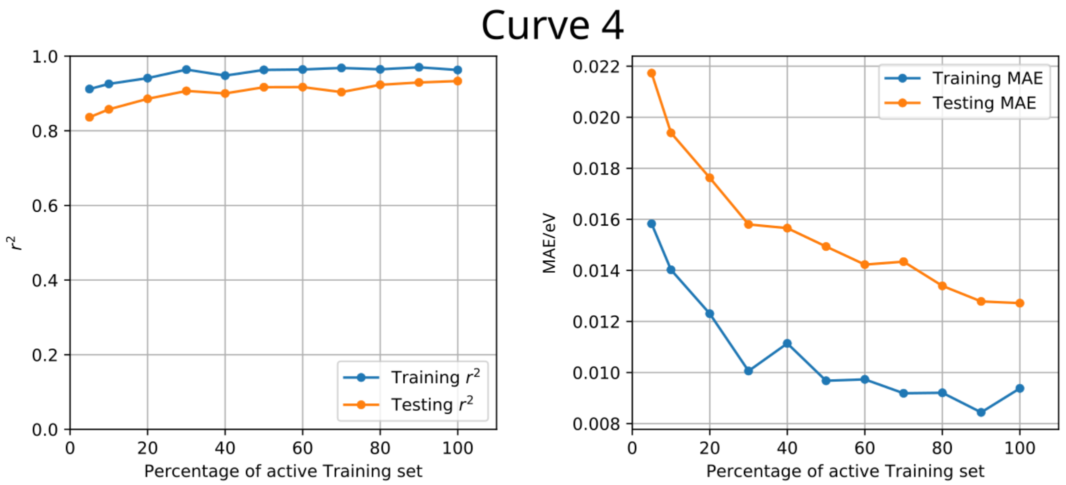
Curve 4
1.0
0.8
0.6
0.4
0.2
0.0
r^2
0
20
40
60
80
100
Percentage of active Training set
Training r^2
Testing r^2
0.022
0.020
0.018
0.016
0.014
0.012
0.010
0.008
MAE/eV
Training MAE
Testing MAE

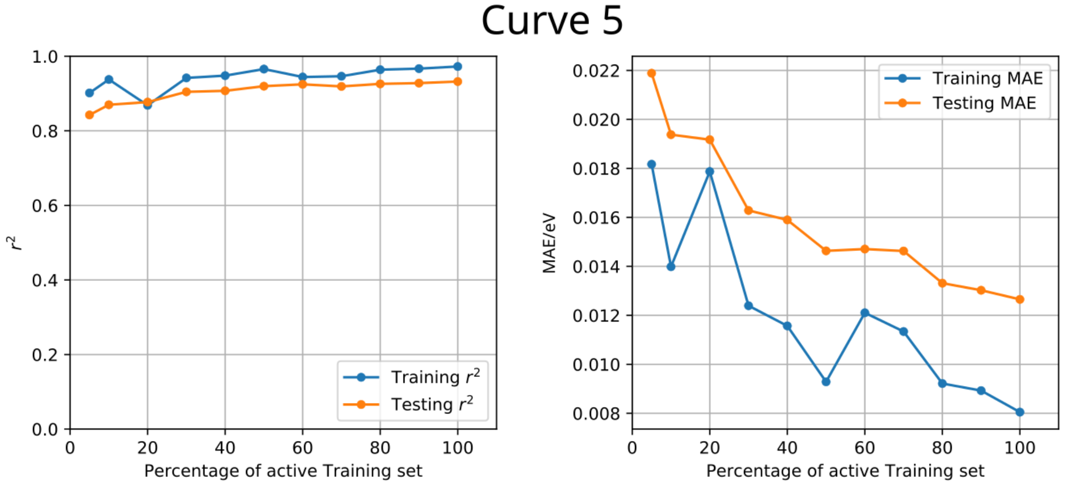
Curve 5
1.0
0.8
0.6
0.4
0.2
0.0
r^2
0
20
40
60
80
100
Percentage of active Training set
Training r^2
Testing r^2
0.022
0.020
0.018
0.016
0.014
0.012
0.010
0.008
MAE/eV
Training MAE
Testing MAE

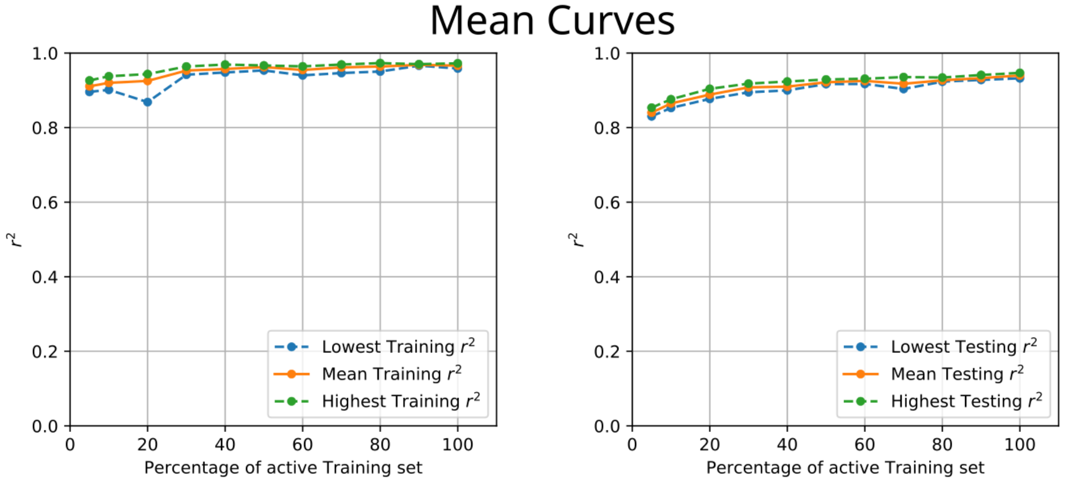
Mean Curves
1.0
0.8
0.6
0.4
0.2
0.0
r^2
0
20
40
60
80
100
Percentage of active Training set
Lowest Training r^2
Mean Training r^2
Highest Training r^2
Lowest Testing r^2
Mean Testing r^2
Highest Testing r^2

S3b: Learning curves for $f(Q_1)$

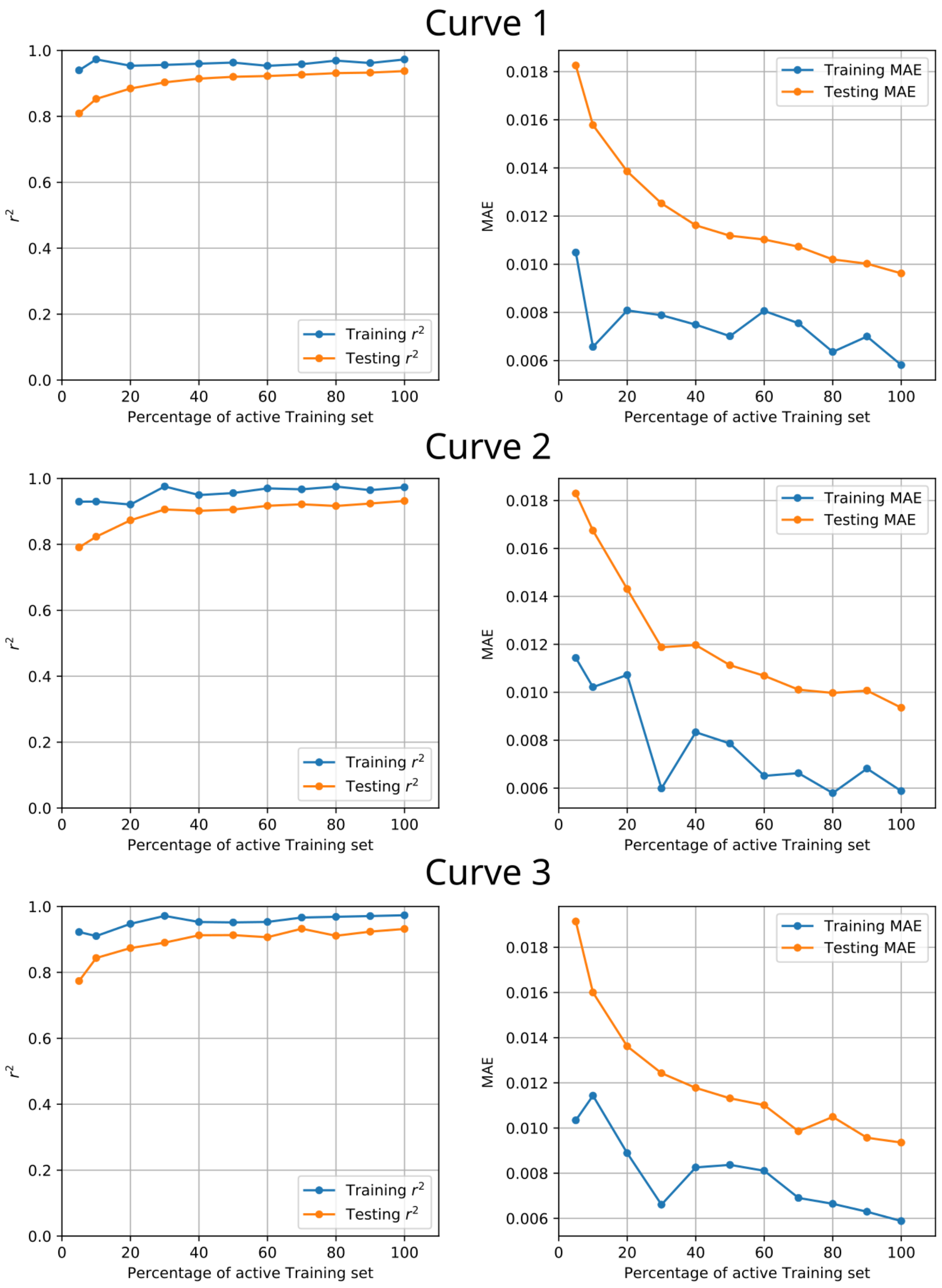

Curve 1

Curve 2

Curve 3

8

Curve 4

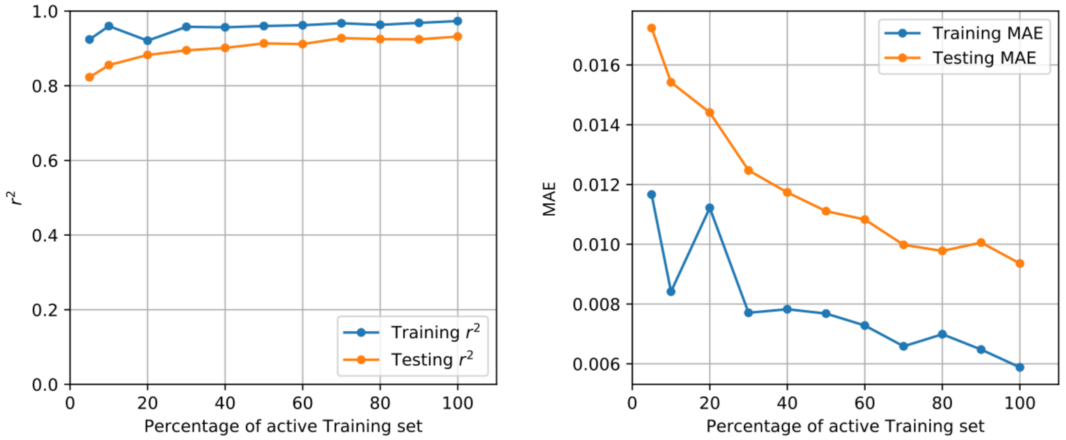

Curve 5

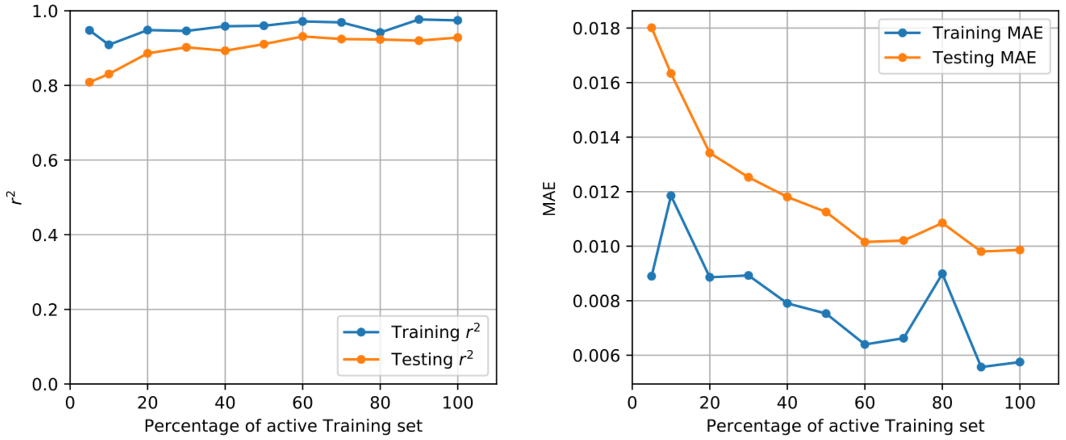

Mean Curves

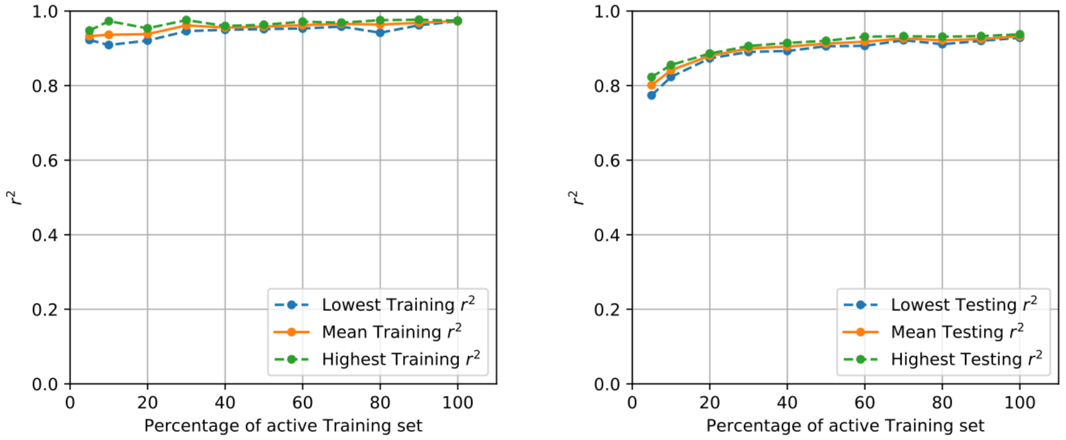

S3c: Learning curves for $\Delta E(Q_2)$

Curve 1

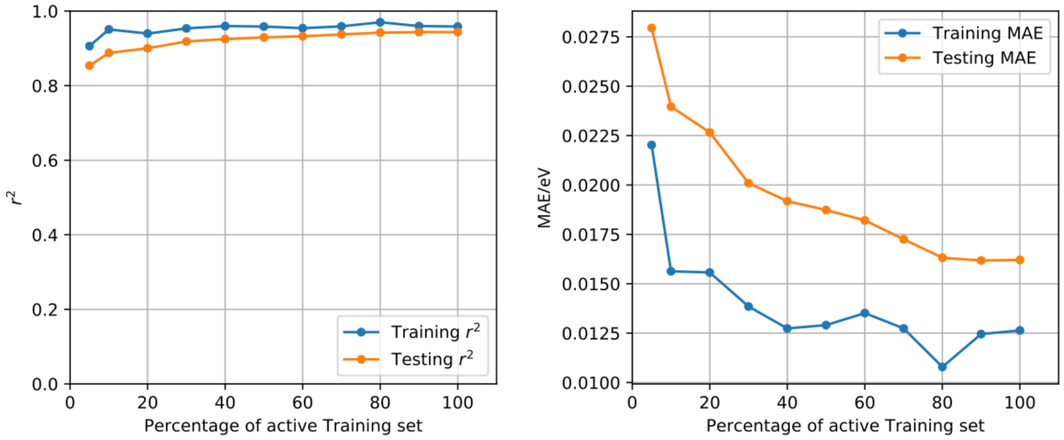

Curve 2

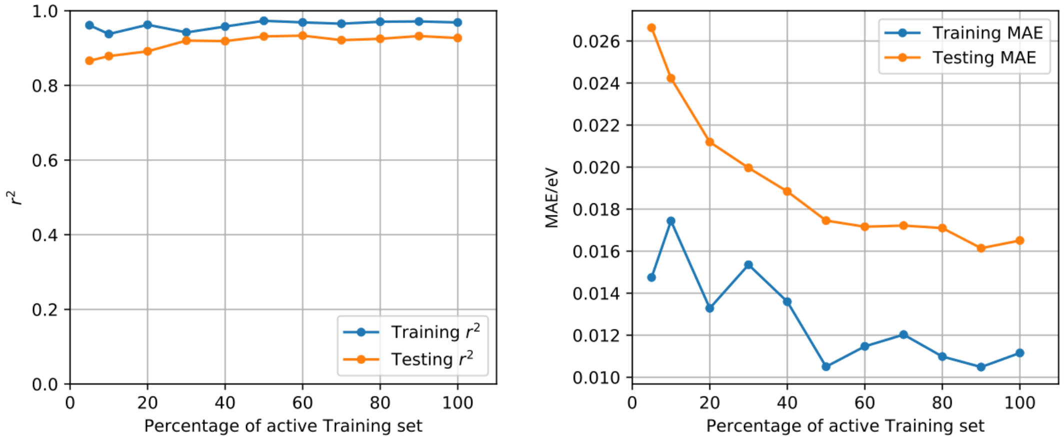

Curve 3

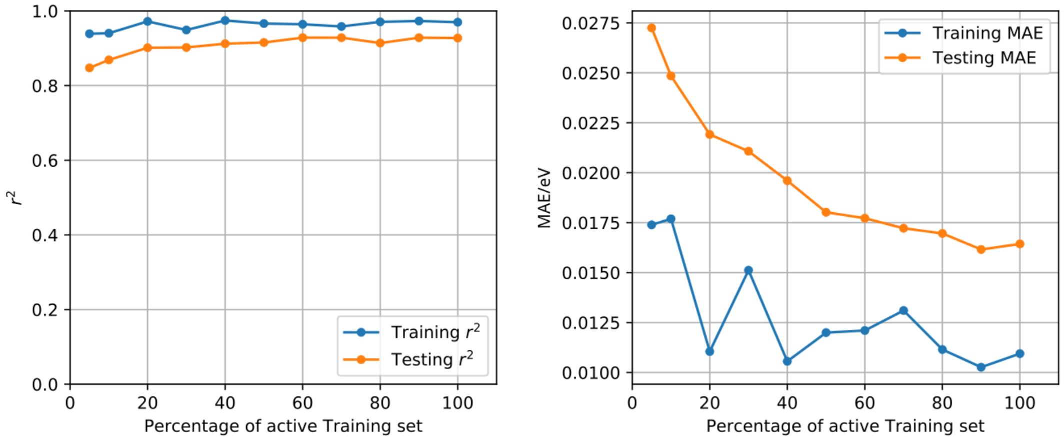

Curve 4

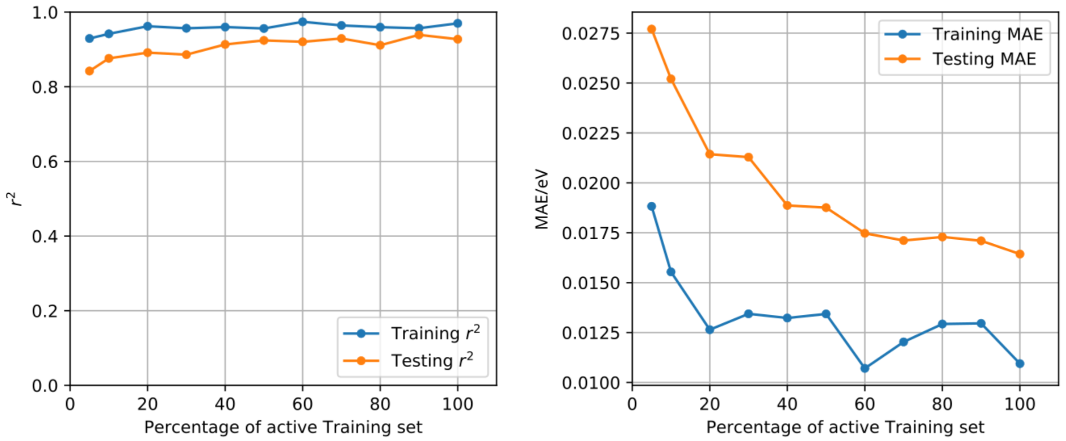

Curve 5

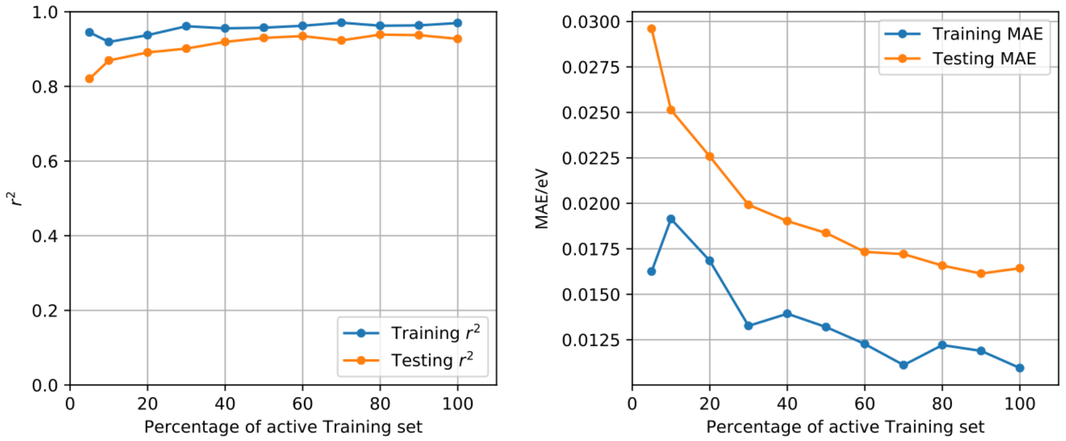

Mean Curves

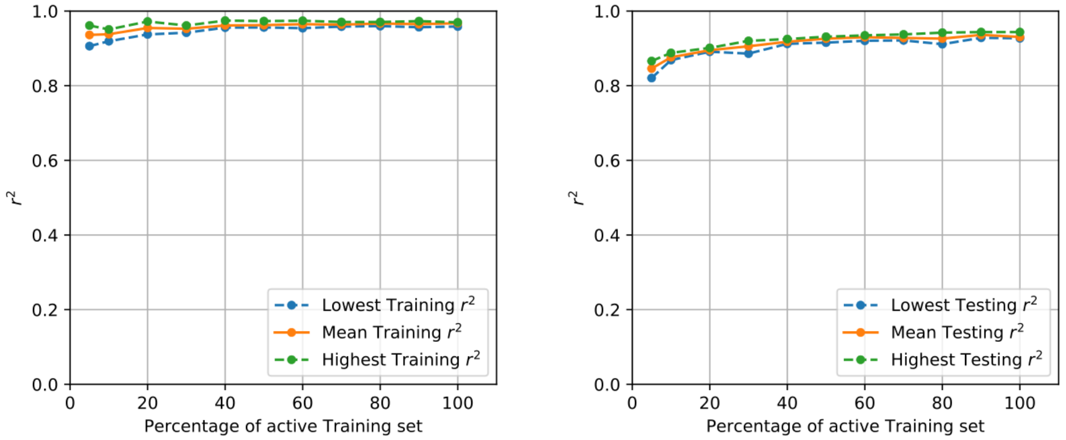

S3d: Learning curves for $f(Q_2)$

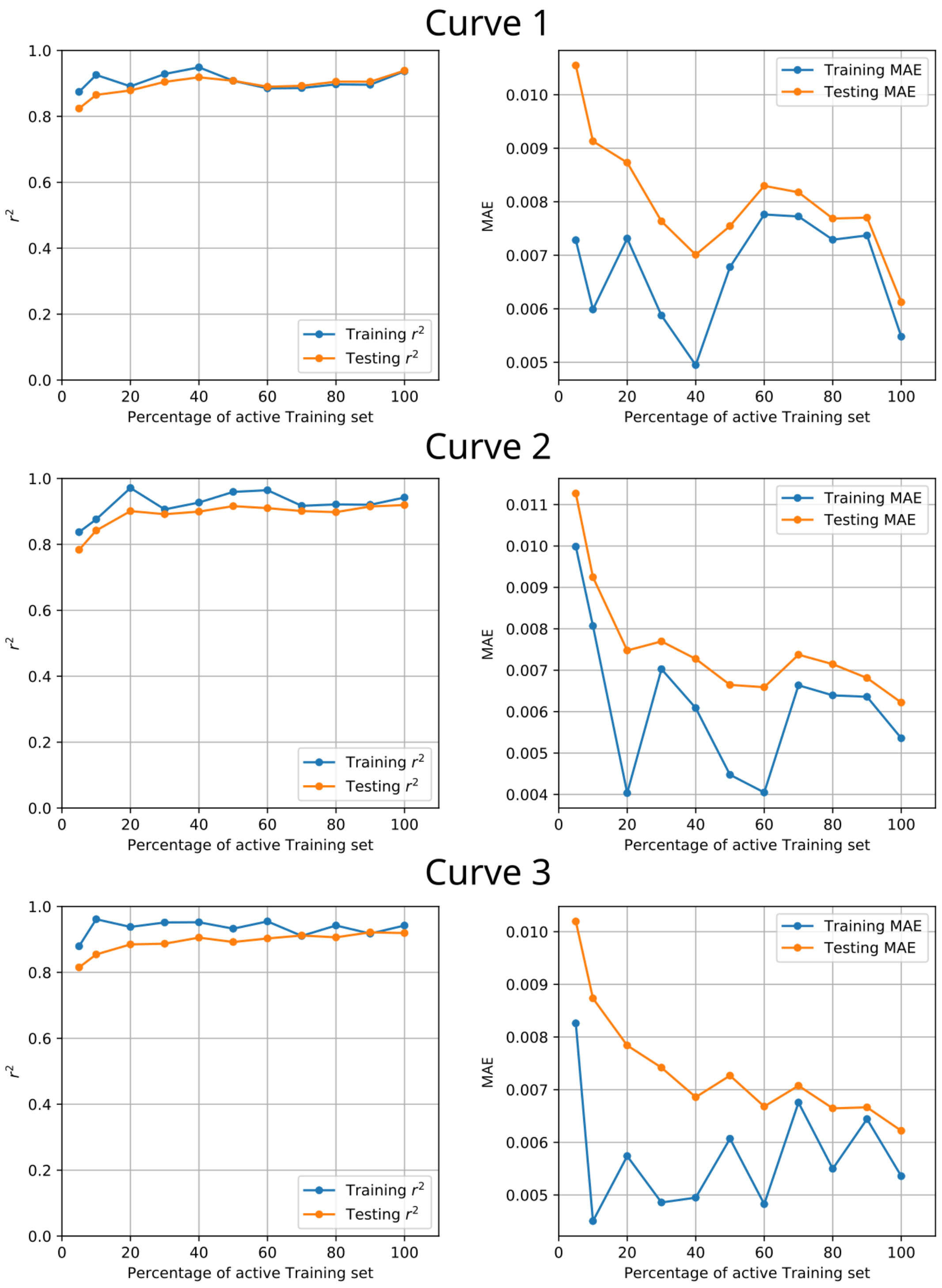

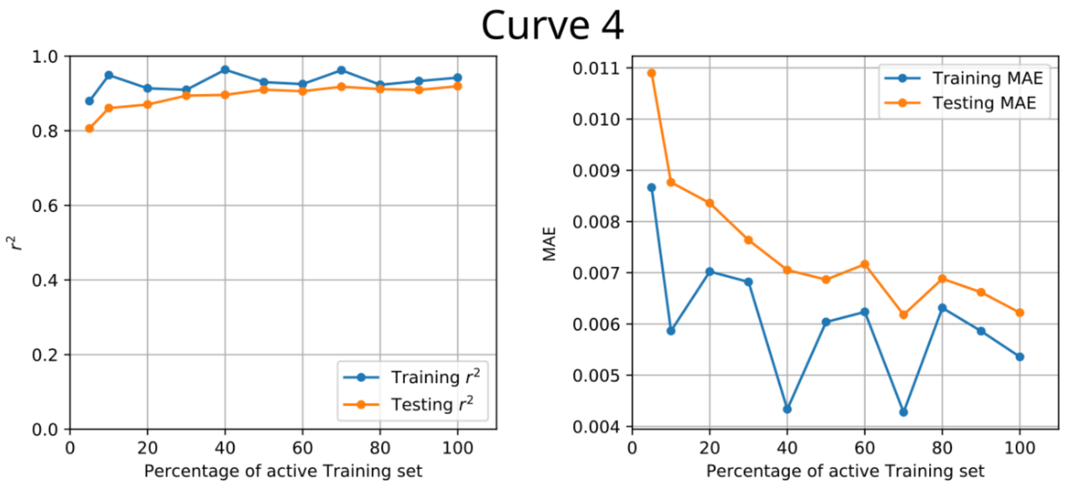
Curve 4
r^2
1.0
0.8
0.6
0.4
0.2
0.0
Training r^2
Testing r^2
MAE
0.011
0.010
0.009
0.008
0.007
0.006
0.005
0.004
Training MAE
Testing MAE
0
20
40
60
80
100
Percentage of active Training set

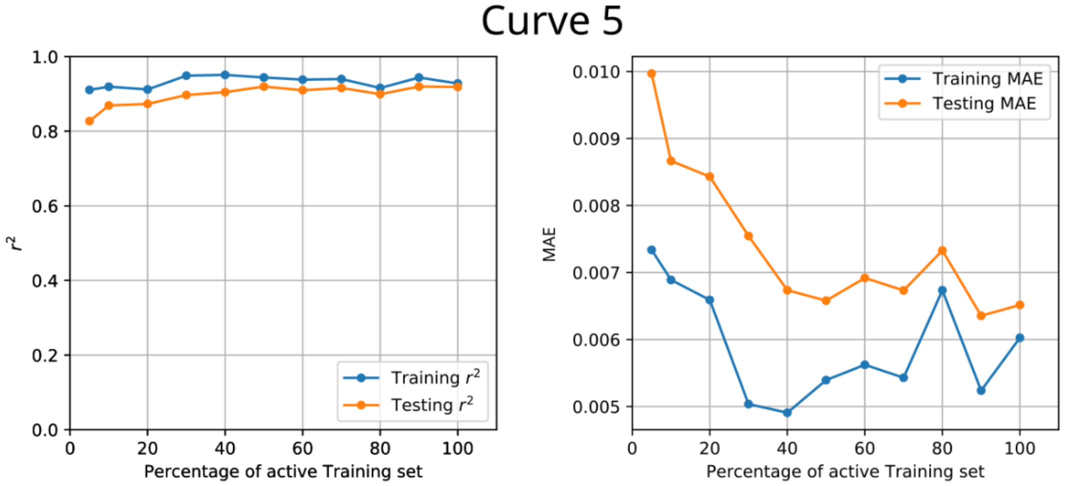
Curve 5
r^2
1.0
0.8
0.6
0.4
0.2
0.0
Training r^2
Testing r^2
MAE
0.010
0.009
0.008
0.007
0.006
0.005
Training MAE
Testing MAE
0
20
40
60
80
100
Percentage of active Training set

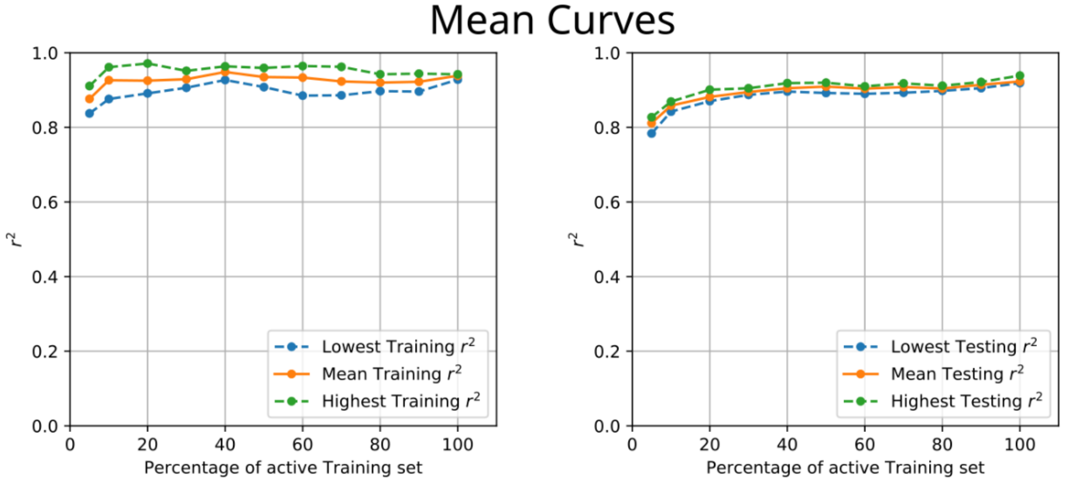
Mean Curves
r^2
1.0
0.8
0.6
0.4
0.2
0.0
Lowest Training r^2
Mean Training r^2
Highest Training r^2
Lowest Testing r^2
Mean Testing r^2
Highest Testing r^2
0
20
40
60
80
100
Percentage of active Training set

S3e: Learning curves for $\Delta E(B_1)$

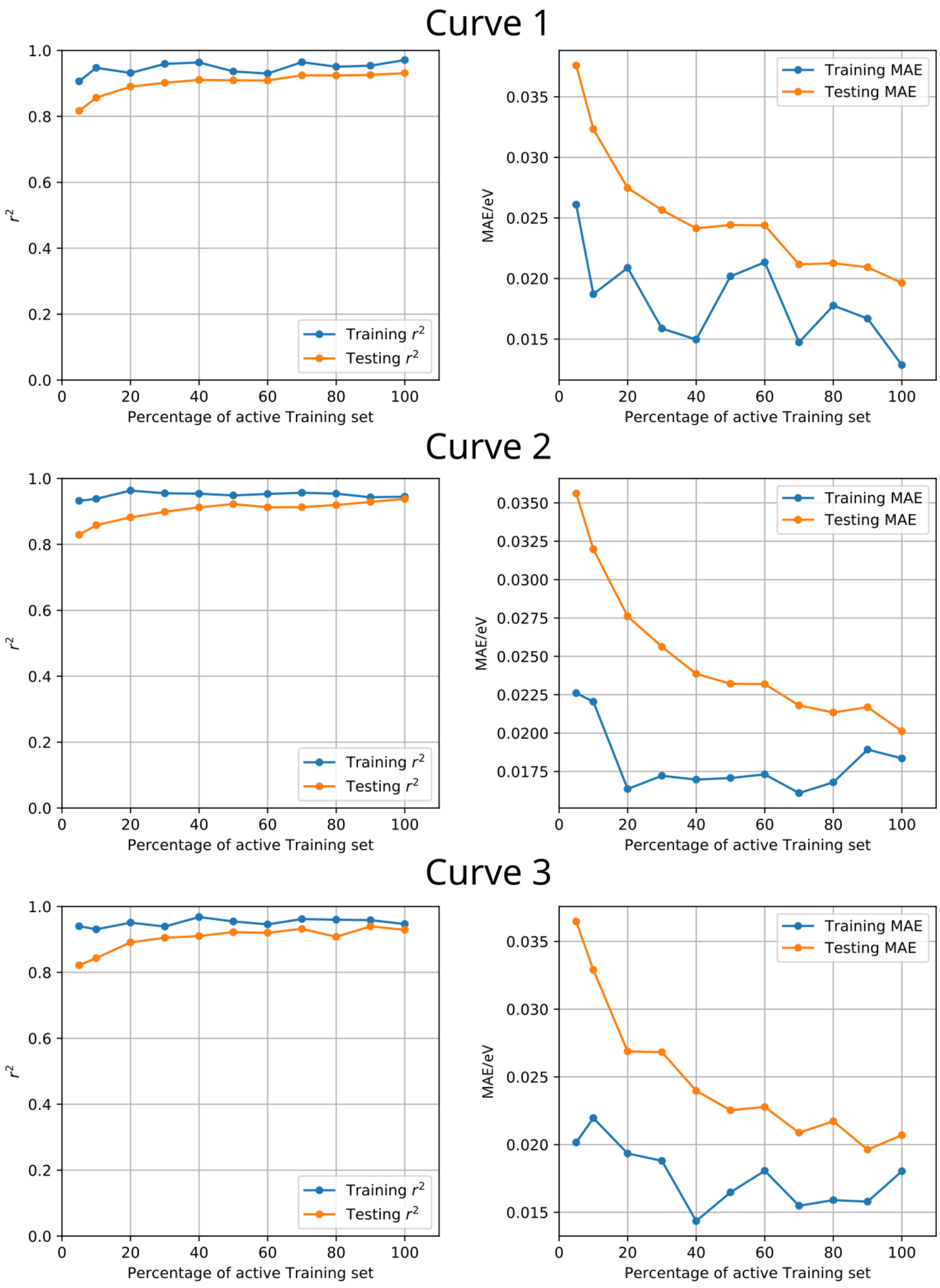

Curve 4

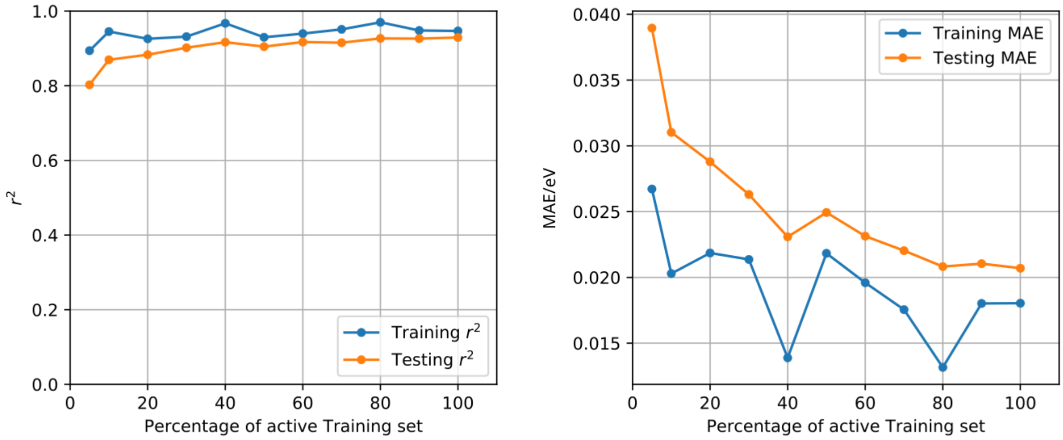

Curve 5

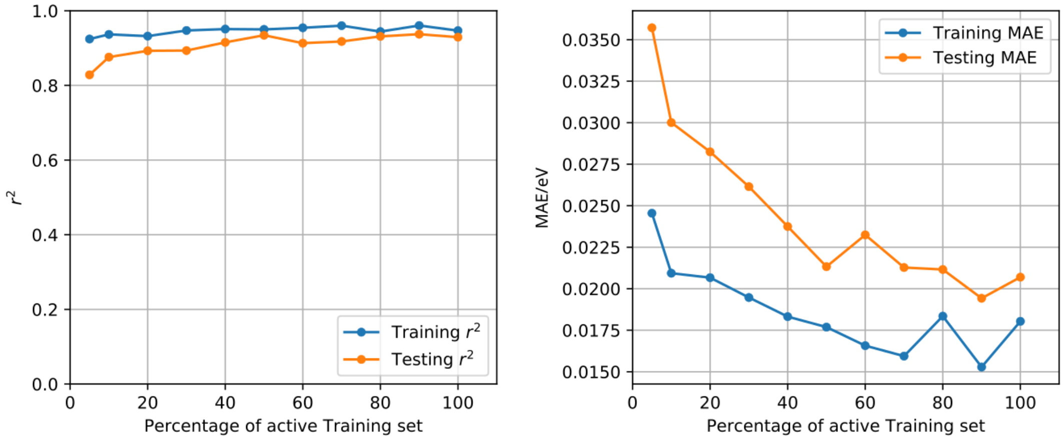

Mean Curves

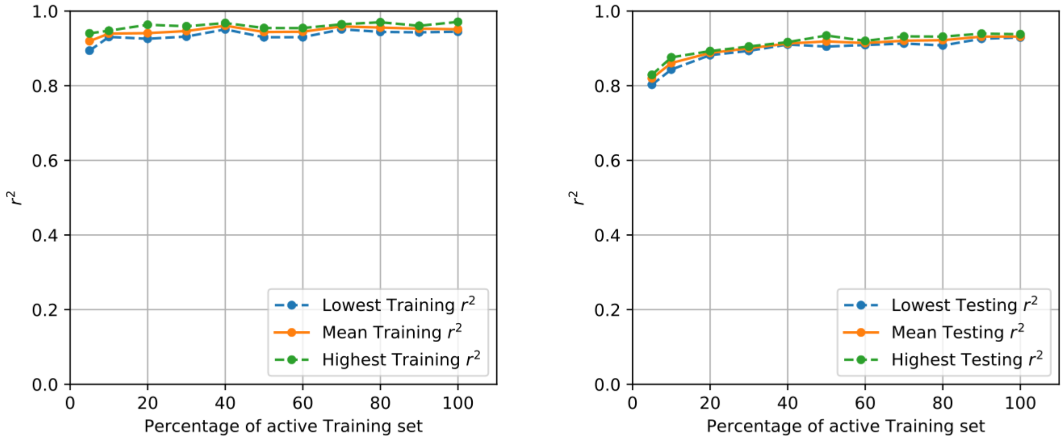

S3f: Learning curves for $f(B_1)$

Curve 1

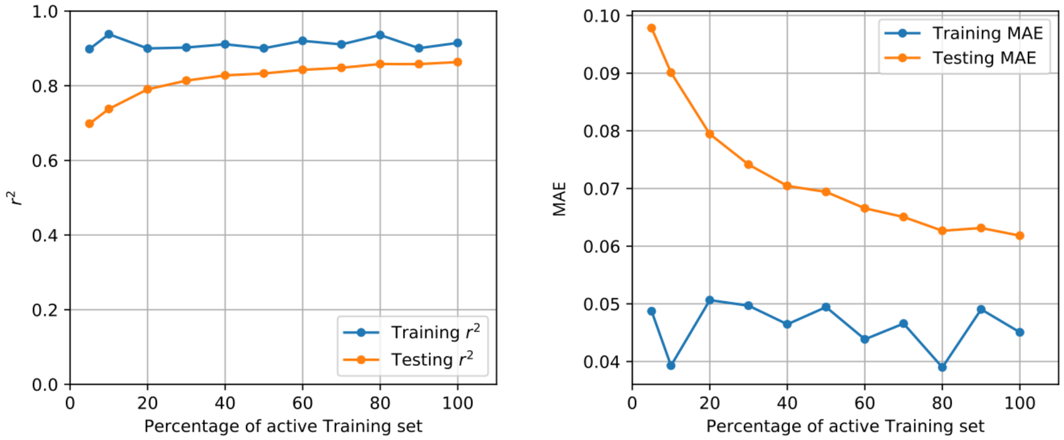

Curve 2

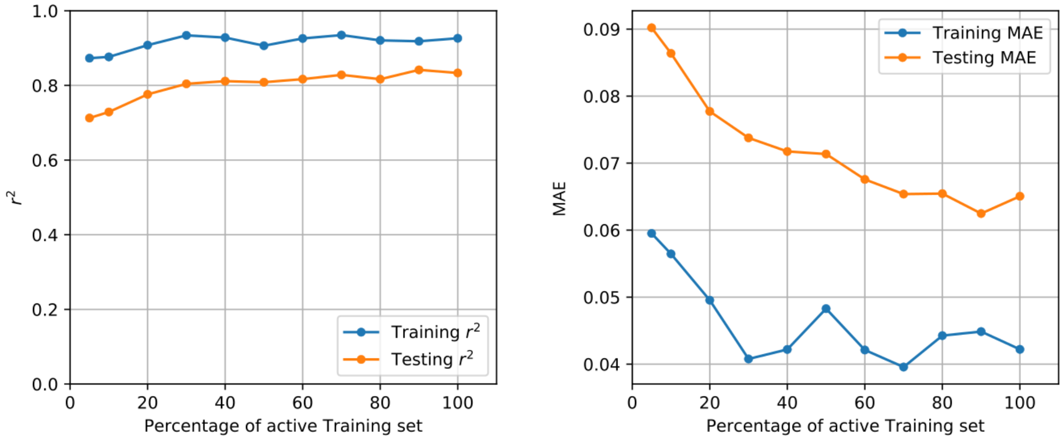

Curve 3

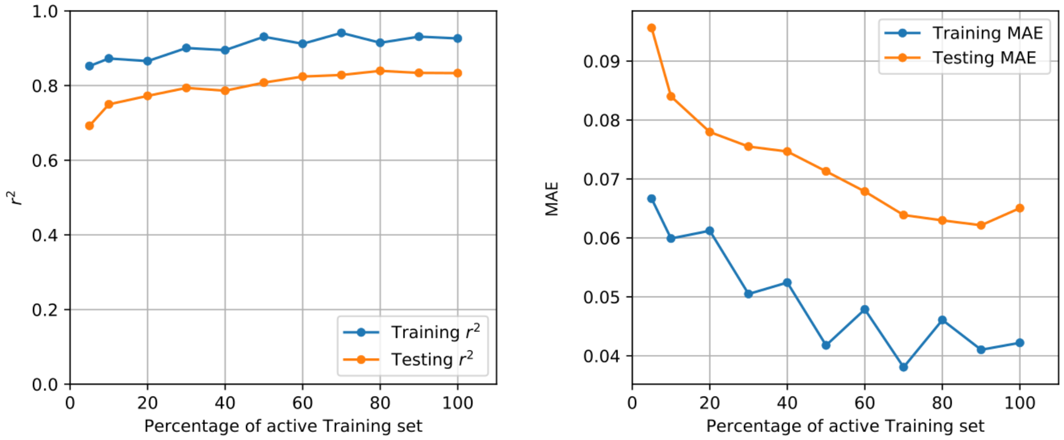

Curve 4

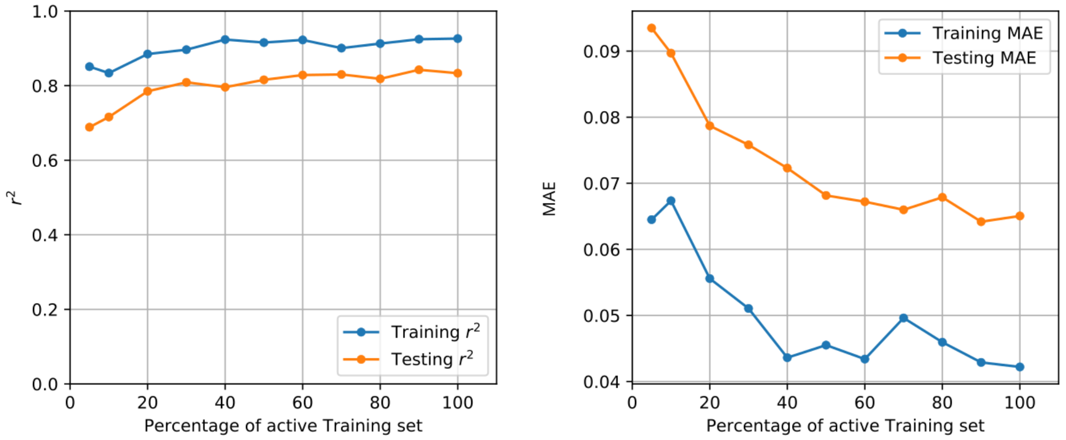

Curve 5

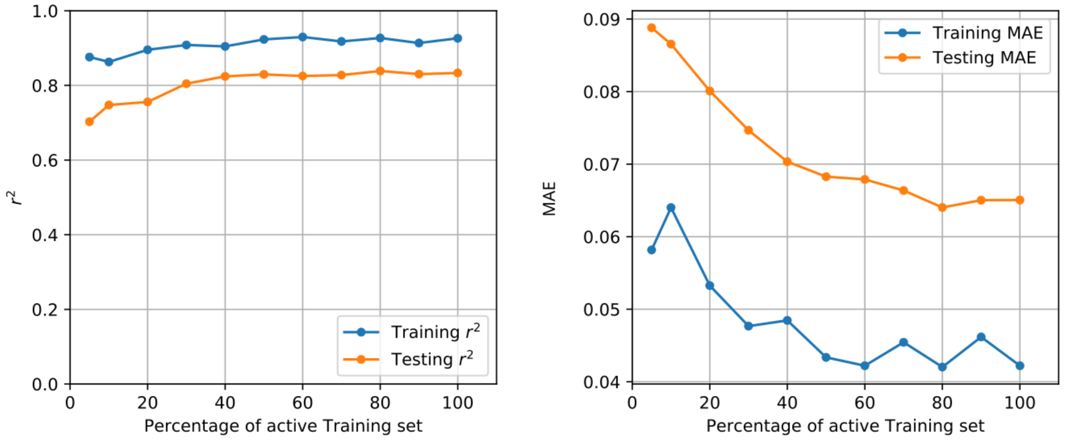

Mean Curves

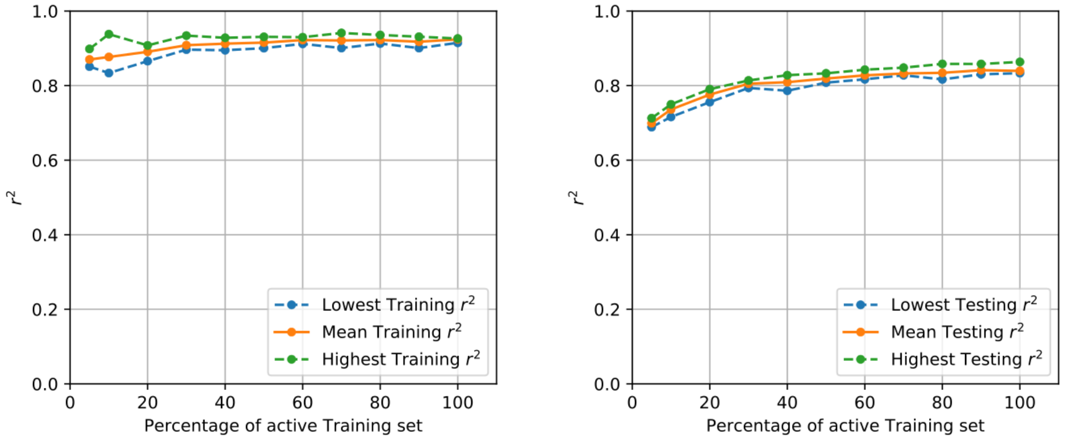

S3g: Learning curves for $\Delta E(B_2)$

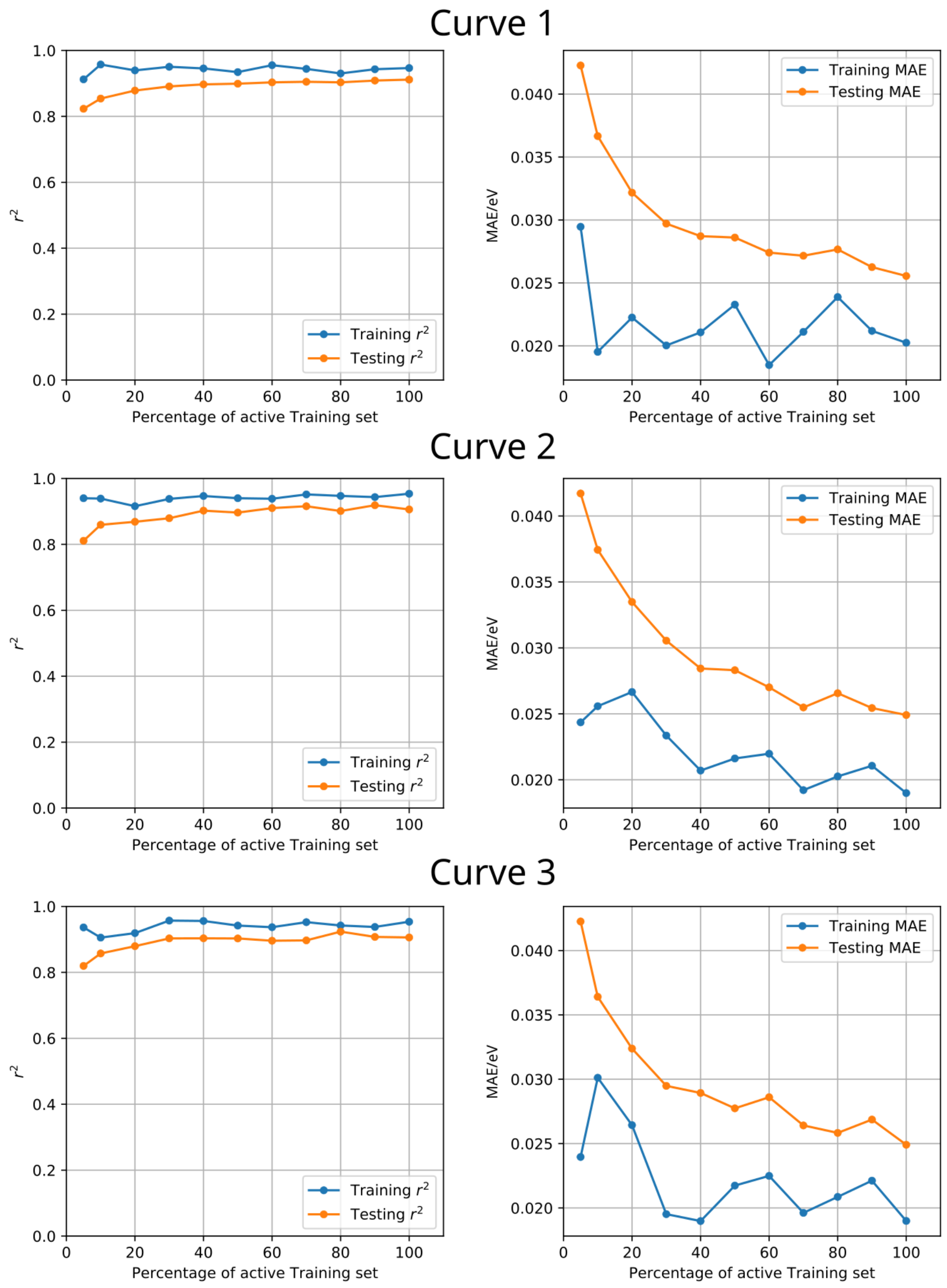

Curve 4

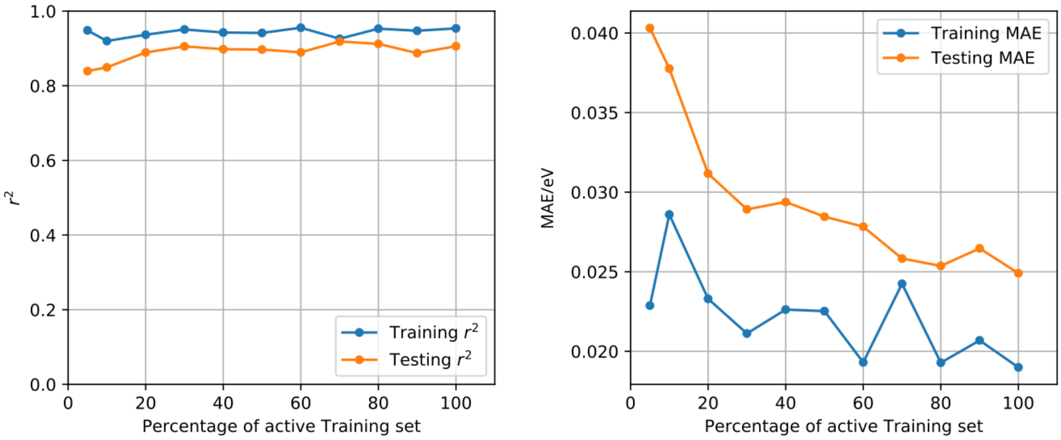

Curve 5

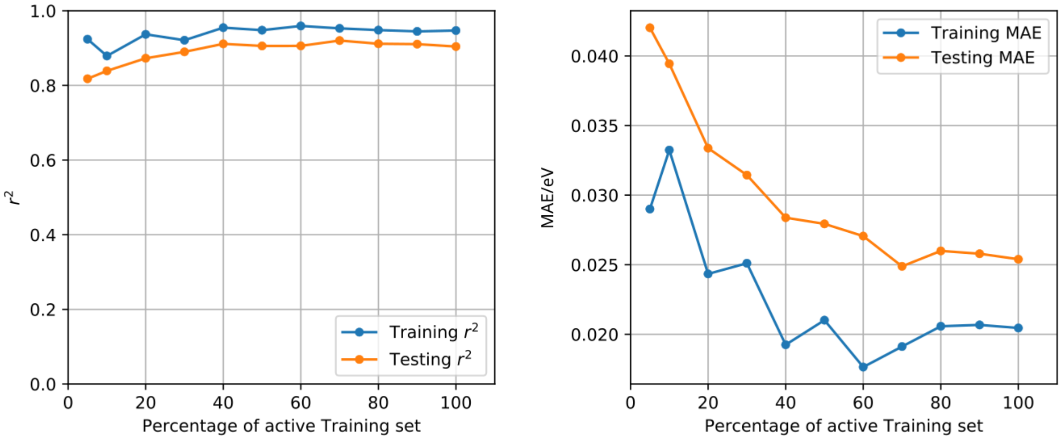

Mean Curves

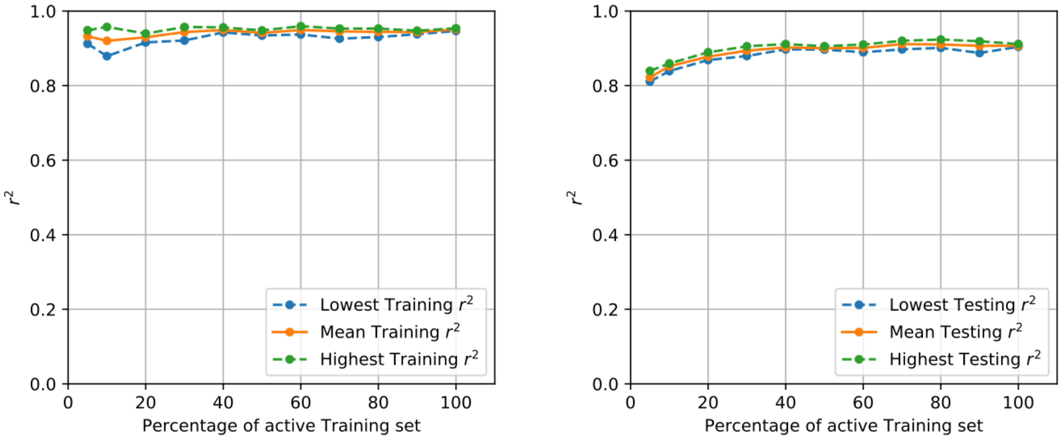

S3h: Learning curves for $f(B_2)$

Curve 1

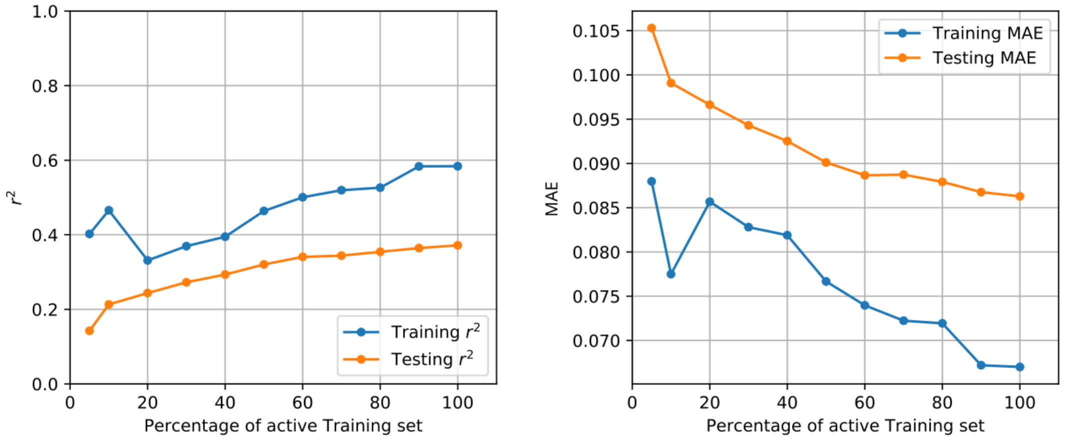

Curve 2

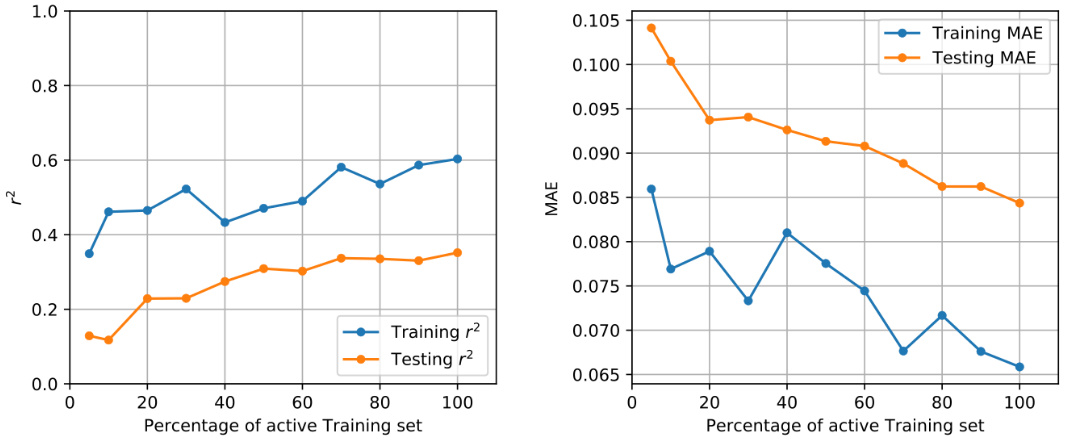

Curve 3

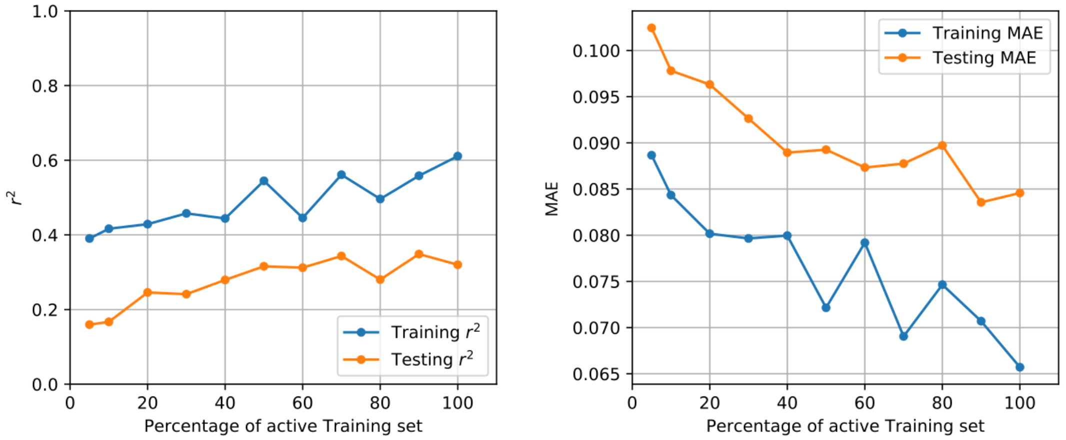

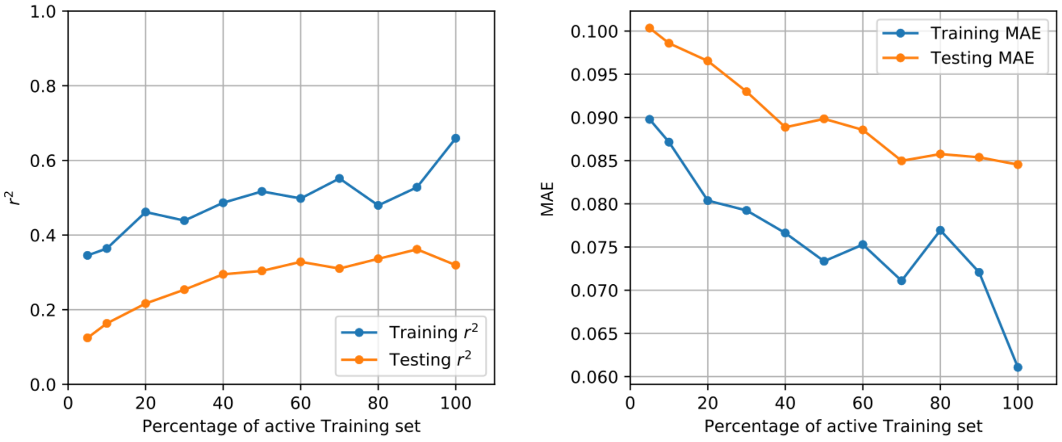
Curve 4

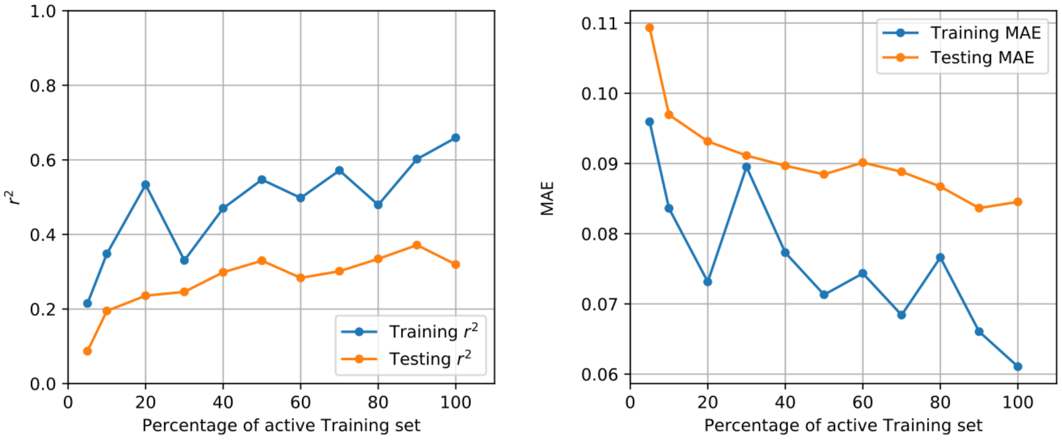
Curve 5

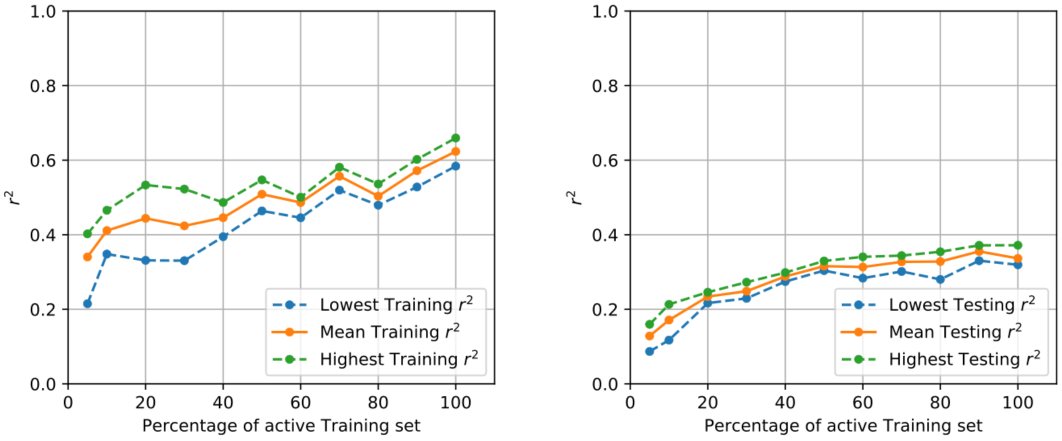
Mean Curves

S3i: Learning curves for $E(T_1)$

Curve 1

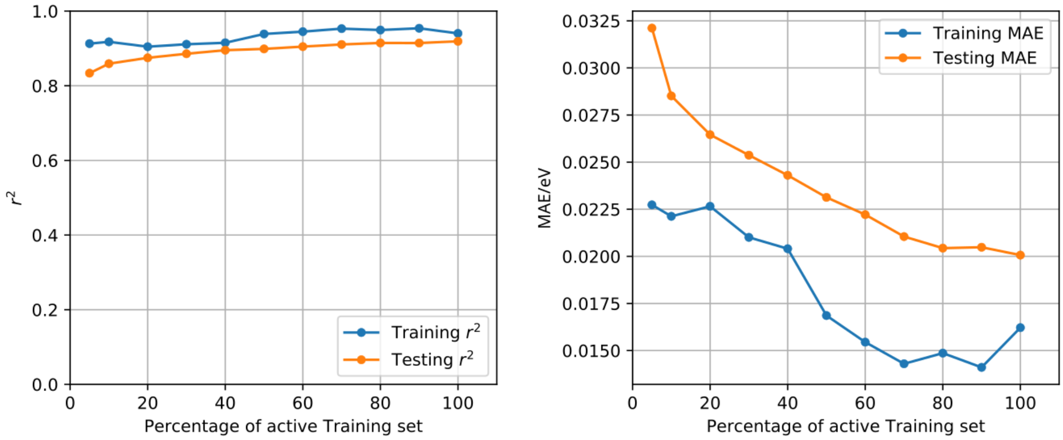

Curve 2

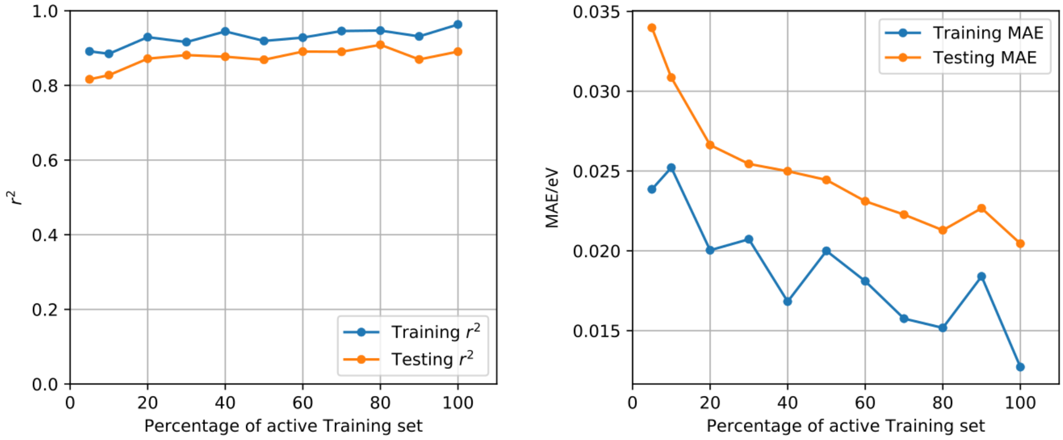

Curve 3

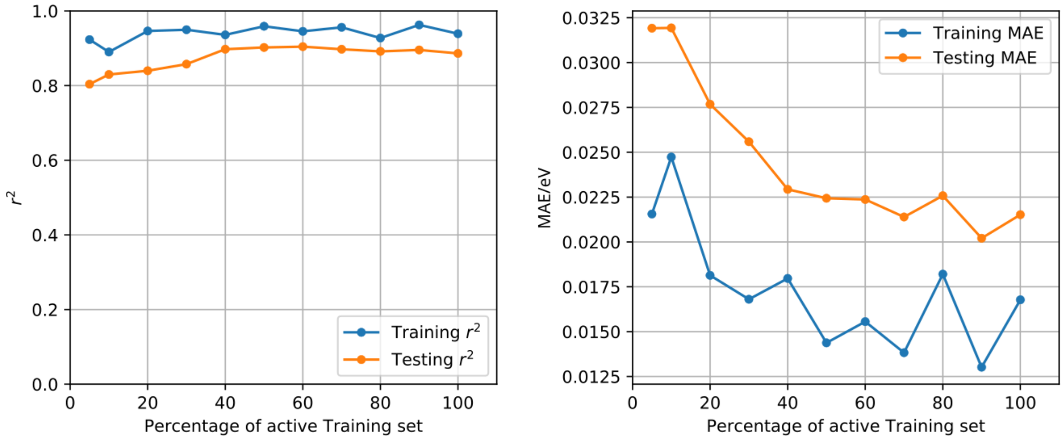

Curve 4

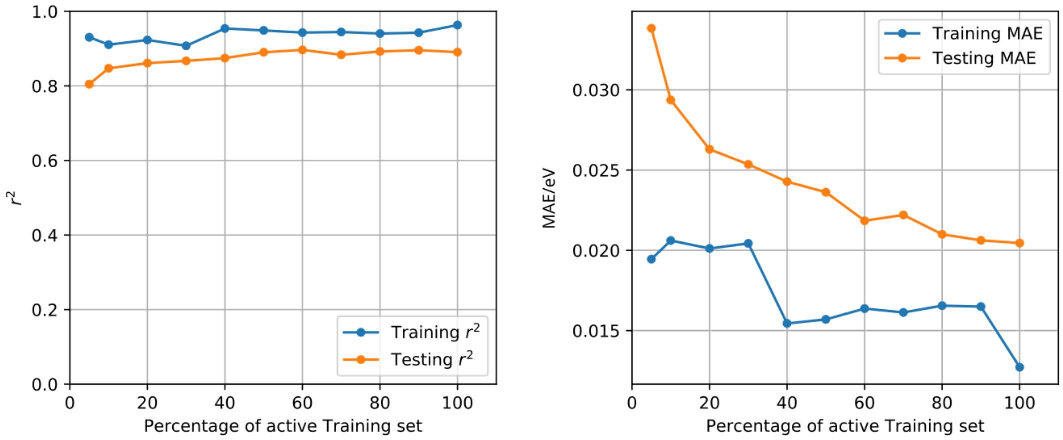

Curve 5

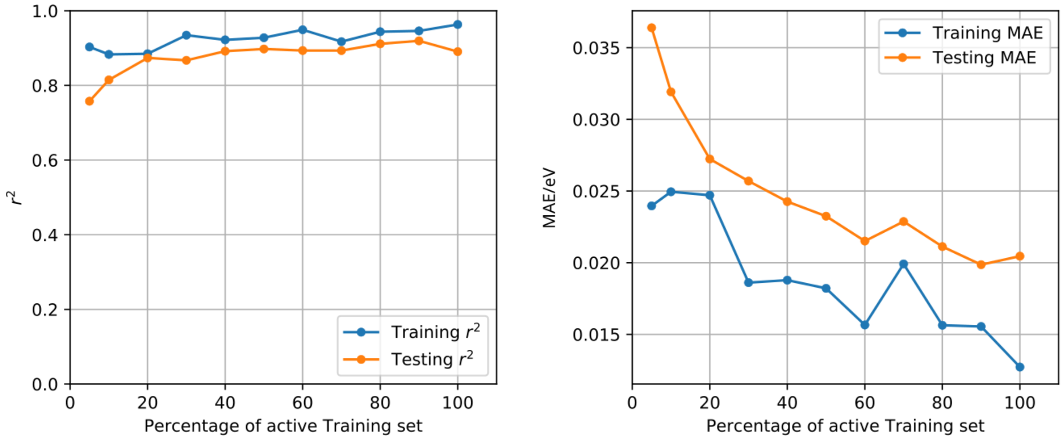

Mean Curves

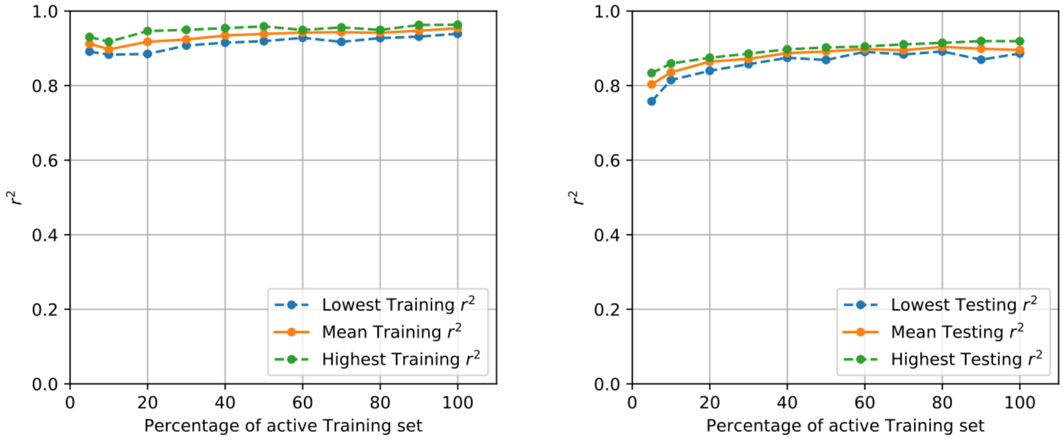

S4: Distribution of training data

Below the distributions of training data for all properties of interest are shown. Each time, pairs of the oscillator strength and respective excitation energy are plotted. For the triplet excitation energy, the x-axis shows the respective $\Delta E(Q_1)$ excitation energies, instead. Note that the red contour lines in all plots show the kernel density estimation for the scattered data, containing 10, 20, 50 and 95% of the data.

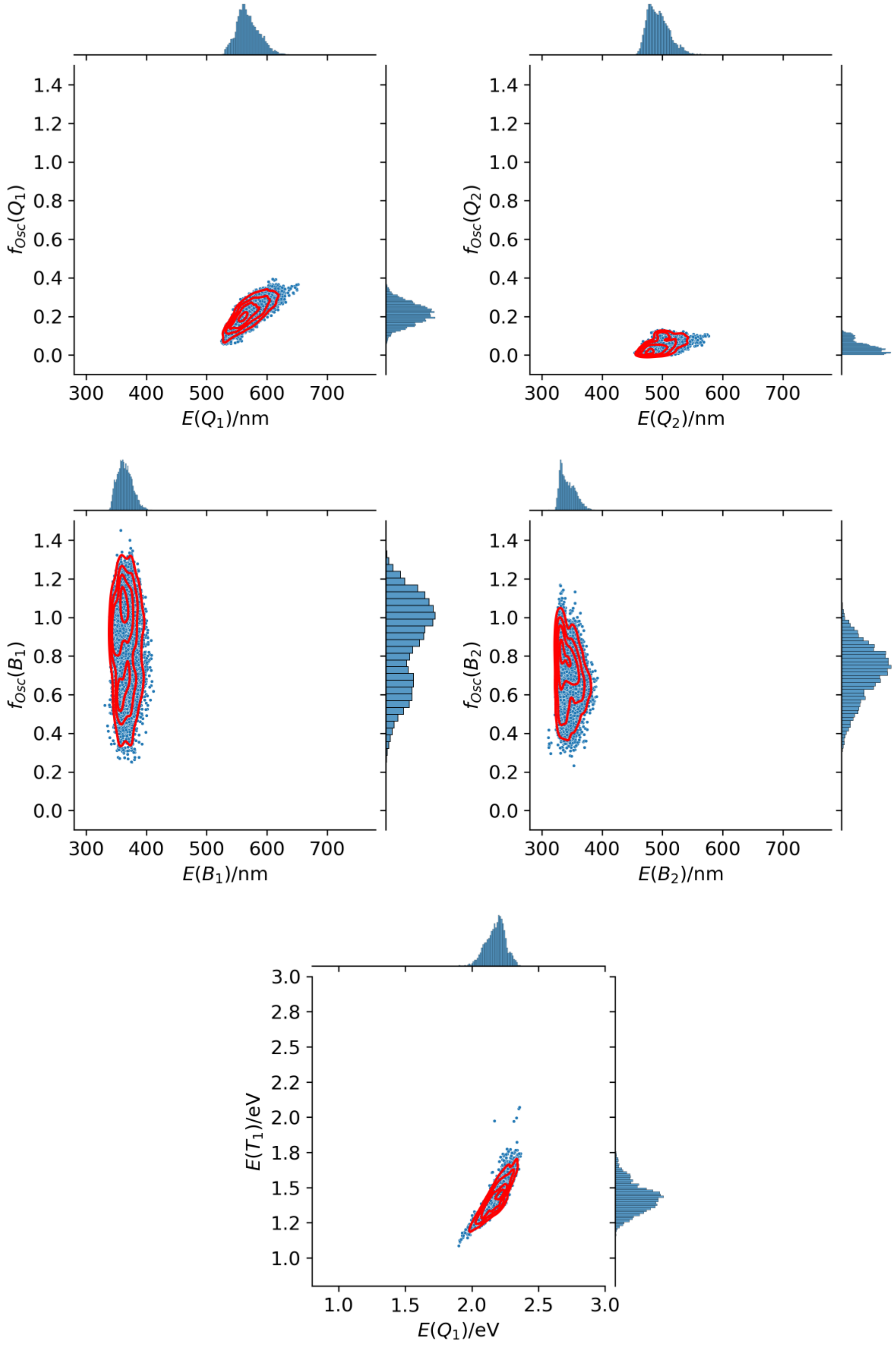

S5: Distribution of prediction data

Below the distributions of prediction data for all properties of interest are shown. Each time, pairs of the oscillator strength and respective excitation energy are plotted. For the triplet excitation energy, the x-axis shows the respective $\Delta E(Q_1)$ excitation energies, instead.

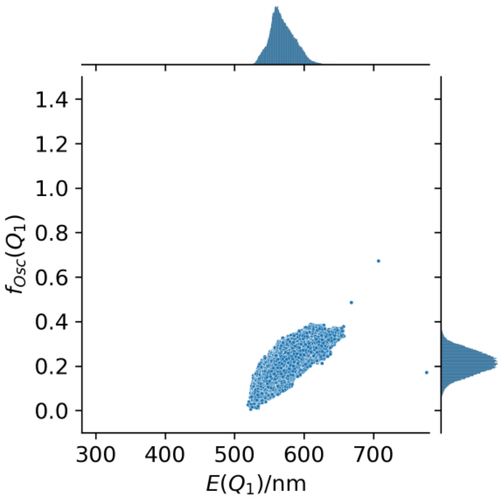

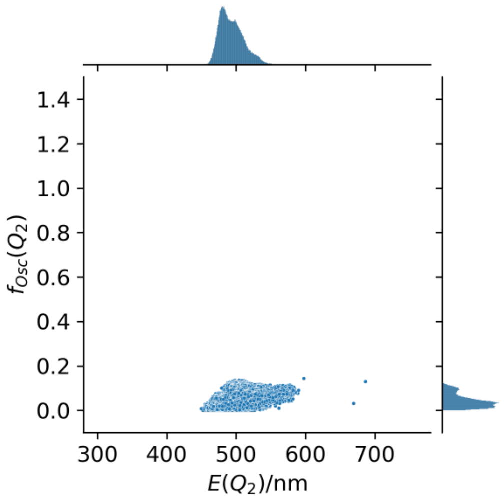

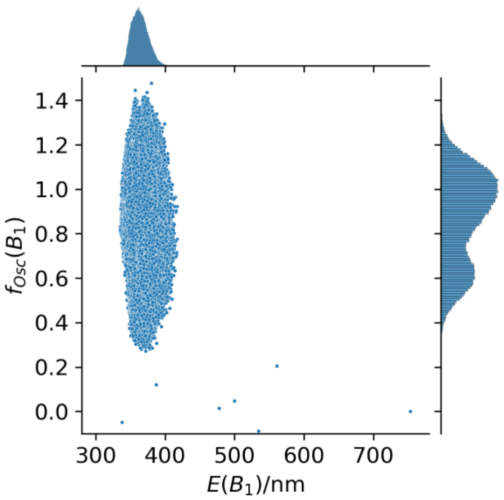

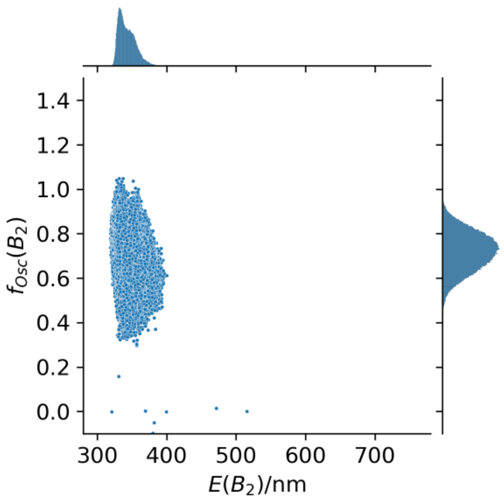

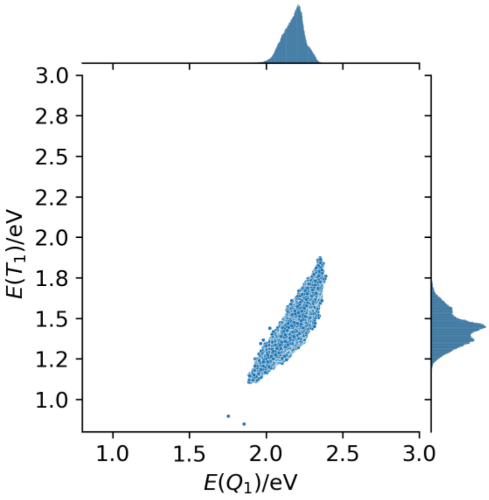

S6: ML procedure, descriptors and ML model applied in this study

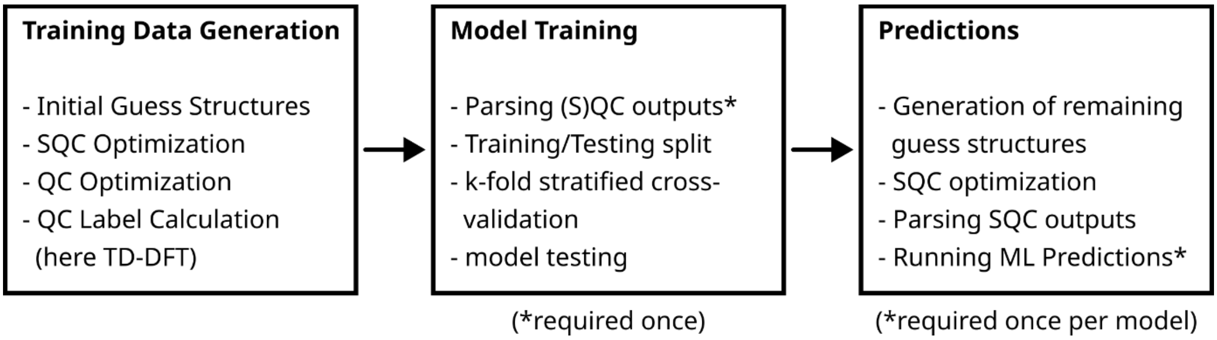

Figure S1: Overview on the full ML procedure, with the individual steps/calculations involved.

Model and descriptors

The predictions provided by ArchOnML are based on Kernel Ridge Regression (KRR) model. A KRR model generates a predicted values E^{pred} for an unknown probe molecule M' by utilizing the expression

$$E^{pred}(M', \boldsymbol{M}) = \sum_i \alpha_i f(M', M_i)$$

Here, α_i are the individual weights when determining the similarity (or kernel) function f between the probe molecule and all molecules that the model was trained on contained in the reference space $\boldsymbol{M}$. Weights α_i are obtained through minimizing the expression

$$\min\ \alpha \sum_i \left(E^{pred}(M', \boldsymbol{M}) - E^{label}\right)^2 + \lambda \sum_i \alpha_i^2$$

where E^{label} are the (TD)-DFT values to be trained against, and λ is the regularization hyperparameter.

The kernel function used in our specific model is of a gaussian type,

$$f(M', M_i) = e^{-\sum_g \left(d_g(M_i, M_j)^2/(2\sigma_g^2)\right)}$$

where d_g is an abstract distance between two molecules M_i and M_j with respect to the g-th descriptor. Further, σ_g constitues a set of gaussian width hyperparameters that are assigned to each individual descriptor. All hyperparameters are optimized through a two-dimensional grid-based 5-fold cross validation procedure. The two dimensions scanned during cross validation concern the parameter λ directly, and a scaling factor $\tilde{\sigma}$ that is applied to initial guess values for σ_g simultaneously. For more details on the procedure, please refer to the documentation of the program code. Finally, note that for each desired property, an individual model was trained using the desired property itself as the argument of stratification.

The following list of keywords defines which descriptors are used to train the KRR models. Note that in ArchOnML, requesting a certain descriptor keyword may produce several separate descriptor values belonging to this type, rather than one value per keyword. This is because some types make use of a user-given variable called **MOWin** - a global variable that determines how many semiempirical orbitals will be considered for these descriptor types. For more details, please refer to the documentation of ArchOnML.With the current settings, a total of 50 descriptors are generated.

Finally, since the used ML model is of KRR type, predictions are formulated by comparing unknown probe molecules to a set of reference molecules. Here, the similarity between molecules is then determined in terms of so-called abstract distances, which are either obtained from just forming the absolute difference of two scalar descriptor values, or by calculation of the Euclidean norm, in case a Coulomb matrix(-like) object is used compare molecules. The original formulation of the latter process can be found in Rupp, M. et al., Phys. Rev. Lett. 108, 058301 (2012). More details on how the similarity between molecules is determined in ArchOnML can be found in the documentation (https://github.com/archonml/archonml).

SEmpNEl This descriptor type uses the individual molecule's number of electrons N_{El}, as is.

SEmpOccs This descriptor type reads the semi-empirical orbital energies for the occupied orbitals E(HOMO−N), with N going up to the specified **MOWin**.

SEmpVirs This descriptor type is the unoccupied (or virtual) space counterpart of **SEmpOccs**. It thus considers the energies of E(LUMO + M), with M going up to **MOWin**.

SEmpEigCoul This descriptor type generates the eigenvalues of a Coulomb matrix, as originally described in Rupp, M. et al., Phys. Rev. Lett. 108, 058301 (2012), as

$$CM_{IJ} = \begin{cases} 0.5Z_I^{2.4}\ for\ I = J \\ \dfrac{Z_I Z_J}{\left|R_I - R_J\right|}\ for\ I\ \neq J \end{cases}$$

Here, matrix elements refer to the I-th and J-th atoms, where Z_I and R_I refer to the atomic number and position in cartesian space of atom I, respectively. The abstract distance between two molecules for this descriptor (and all other Coulomb matrix-like descriptors) is calculated as the aforementioned Euclidean norm between the eigenvalues of two different molecules M_i and M_j according to

$$d_{EigCoul}(M_i, M_j) = \sqrt{\textstyle\sum_I \left|\epsilon_I^i - \epsilon_I^j\right|^2},$$

where ϵ_I is the I-th eigenvalue of the specific molecule M_i or M_j, sorted in descending order. Note, that in case there is a difference in the number of atoms between M_i and M_j, the shorter array is supplemented by zeros.

SEmpOccEigCoul This descriptor type makes use of a Coulomb matrix-like object, in which the atomic charges of the original Coulomb matrix in the mixing terms are additionally multiplied with the amount of Mulliken charge q_I at each atom I.

SEmpOccPCMEigCoul This descriptor constructs a Coulomb matrix-like object that additionally considers the so-called p-orbital character of an occupied orbital HOMO-N at each specific atom I (or J, likewise). Here, p-orbital character $p_I(N)$ is quantified abstractly as the sum of coefficients of atomic orbitals' p-character at each specific atom for the specific molecular orbital HOMO-N, thus becoming an orbital shape descriptor.

$$p_I(N) = p_{I,x}(N) + p_{I,y}(N) + p_{I,z}(N)$$

Here, $p_{I,x}$ gives the sum of all atomic orbital coefficients at atom I of p_x character, and N stands for the HOMO-N orbital. The other cartesian components are summed up and added. Ultimately, the Coulomb matrix-like object is then defined as

$$CM_{IJ}^{p-char}(N) = \begin{cases} 0.5\left|Z_I p_I(N)\right|^{2.4}\ for\ I = J \\ \dfrac{(\left|Z_I p_I(N)\right|)(\left|Z_J p_J(N)\right|)}{\left|R_I - R_J\right|}\ for\ I\ \neq J \end{cases}$$

Note that this descriptor is affected by **MOWin**, thus considering occupied orbitals HOMO-N up to N = **MOWin**. When constructing the abstract distances, only identical orbital indices are compared, applying the same sorted Euclidean norm formalism introduced earlier.

SEmpVirPCMEigCoul This descriptor is the analogue of **SEmpOccPCMEigCoul**, that considers unoccupied orbitals instead. It also considers multiple orbitals using **MOWin**.

SEmpHOLUPDiff This descriptor keyword requests construction of Coulomb matrix-like objects that consider local electron density differences of p-orbital type between only the HOMO and LUMO. Here, "p-orbital character density difference at atom I with respect to HOMO and LUMO" D_I is calculated as the difference of squared, local p-orbital characters according to

$$D_I(M=0,N=0)=p_I(M=0)^2-p_I(N=0)^2$$

The Coulomb matrix-like object is then defined as

$$CM_{IJ}^{p-diff}=\begin{cases}0.5|Z_I D_I(M=0,N=0)|^{2.4}\; for\; I=J\\ \dfrac{(|Z_I D_I(M=0,N=0)|)\left(|Z_J D_J(M=0,N=0)|\right)}{|R_I-R_J|}\; for\; I\neq J\end{cases}$$

SEmpOrbEnDiffs This descriptor compares semiempirical orbital energy differences in eV between occupied orbital HOMO-N and virtual orbital LUMO+M.

$$E_{Diff}(M,N)=E(LUMO+M)-E(HOMO-N)$$

When calculating the abstract distance for a pair of molecules M_i and M_j, it will only compare same-index-pairs. In other words, it will only compare the energy differences of a certain HOMO-N to LUMO+M transition in both molecules – but never use different orbital indices.

SEmpTransPCMEigCoul This descriptor type abstractly expresses a transition moment between orbitals HOMO-N and LUMO+M by multiplying local p-characters of the two orbitals at atoms I and forming a Coulomb matrix-like object out of it. This so-called local transition contribution $T_I(M, N)$ at atom I for orbitals HOMO-N and LUMO+M is then defined as

$$T_I(M,N)=p_I(M)*p_I(N)$$

and the corresponding matrix expression is constructed as

$$CM_{IJ}^{T}(M,N)=\begin{cases}0.5(|Z_I T_I(M,N)|)^{2.4}\; for\; I=J\\ \dfrac{(|Z_I T_I(M,N)|)\left(|Z_J T_J(M,N)|\right)}{|R_I-R_J|}\; for\; I\neq J\end{cases}$$

Again only same-index pairs for N and M are considered in the Euclidean norm.

SEmpOccVirPTransSum This descriptor keyword requests the summation of all atomic contributions of the above-defined p-character transition densities at each atom I between orbital pairs HOMO−N and LUMO+M in scalar form according to

$$TS(M,N)=\sum_I|T_I(M,N)|^2.$$

The abstract distance between molecules for this sum of local transitions is obtained as the simple absolute difference of the scalar values.

S7: Criterion for B band state selection in the ML scheme

For the evaluation of the Soret band, the two excited states with the highest oscillator strengths were selected, after exclusion of the S_1 (= Q_y) and S_2 (= Q_x) state transitions. To avoid selecting an unrealistic state that has a high f, but also a transition energy outside of the B band, an additional selection criterion was based on the cumulative oscillator strength: the sum of all considered states' f was tracked, and once this sum exceeded a value of 4, no further states were considered. This ensured a focused analysis on the most intense transitions contributing to the Soret band, while maintaining a consistent basis for comparison.

S8: Comparison of ML data to conventional QC: TD-DFT (gas phase and acetone)

Q band shifts

Table S1: Vertical excitation energies (in eV) and oscillator strengths of the first electronic transition (S_0→S_1) for various Q red-shifted Chls, from different theoretical models. For the artificial Chls, difference to Chl f is given in parentheses.

	Model	Chl *f*	Chl *df*	Chl *f+*
ΔE_{0-S1} / eV	Pred. (vac.)	2.068	2.047 (-0.021)	2.045 (-0.023)
	TD-DFT (vac.)	2.250	2.239 (-0.011)	2.241 (-0.009)
	TD-DFT (acetone)	2.136	2.158 (+0.022)	2.196 (+0.060)
f_{0-S1}	Pred. (vac.)	0.31	0.32 (+0.01)	0.36 (+0.05)
	TD-DFT (vac.)	0.42	0.41 (-0.01)	0.47 (+0.05)
	TD-DFT (acetone)	0.63	0.63 (±0.00)	0.63 (±0.00)

The gas phase TD-DFT calculations shown in Table S1 agree well with the KRR predictions. However, calculations in acetone imply a sensitivity regarding the first excited state, especially for ΔE_{0-S1}. Instead of shifting slightly down in energy, TD-DFT computes the new variants as shifted up compared to Chl f. Comparing the vacuum and acetone values shows that TD-DFT predicts Chl *f* to be more affected by the presence of the solvent than the suggested Chl variants (about 120 meV shift compared to 80 or 50 meV for the new variants). The actual shift can thus be considered to be dependent on the present environment.

B band shifts

Table S2: Vertical excitation energies (in eV) and oscillator strengths of the selected B band electronic transition (S_0→S_X) for various B red-shifted Chls, from different theoretical models. For the artificial Chls, difference to Chl b is given in parentheses. Values in italics correspond to X = 3, as here, the selected X was different; only applies to TD-DFT in gas phase.

	Model	Chl *b*	DVChl *b*	Chl *bb*	Chl *bd*
ΔE_{0-SX} / eV	Pred. (vac.)	3.378	3.218 (-0.160)	3.222 (-0.156)	3.288 (-0.090)
	TD-DFT (vac.)	3.846 *3.695*	3.592 (-0.254) */ (-0.103)*	3.583 (-0.263) */ (-0.112)*	3.663 (-0.183) *3.548 (-0.147)*
	TD-DFT (acetone)	3.446	3.315 (-0.131)	3.278 (-0.168)	3.364 (-0.082)
f_{0-SX}	Pred. (vac.)	1.04	1.23 (+0.19)	1.09 (+0.05)	1.07 (+0.03)
	TD-DFT (vac.)	1.54 *0.86*	1.40 (-0.14) */ (+0.54)*	1.49 (-0.05) */ (+0.63)*	1.34 (-0.20) *0.85 (-0.01)*
	TD-DFT (acetone)	1.75	1.99 (+0.24)	1.73 (-0.02)	1.88 (+0.13)

As noted above, the state identification issue mentioned above and in the main article affects the interpretation of the B band states in Table S2. TD-DFT generally predicts two or more states with significant (more than 0.5) oscillator strengths, and both the predictions and acetone models agree that usually the lowest B band state (S_3) is a bright/the brightest state, respectively. The values in italics indicate those cases for which S_3 was *not* the one with highest f, which only applies to TD-DFT in vacuum. When neglecting the vacuum TD-DFT calculations and their more difficult state assignment, we can see that the ML predictions nicely agree with the TD-DFT/acetone calculations, both for energies and oscillator strengths.

S8, continued

Triplet-shifted Chl variants

Table S3: Vertical energy differences between the S_0, S_1 and T_1 states (in eV) for various Chls with ΔE_{0-S1} close to that of Chl a, but with shifted triplet energies, from different theoretical models. For the artificial Chls, difference to Chl a is given in parentheses.

	Model	Chl *a*	3Ac-Chl+	DVChl *bf*
ΔE_{0-S1} / eV	Pred. (vac.)	2.144	2.151 (-0.007)	2.153 (+0.009)
	TD-DFT (vac.)	2.358	2.350 (-0.008)	2.305 (-0.053)
	TD-DFT (acetone)	2.316	2.320 (+0.004)	2.258 (-0.058)
ΔE_{0-T1} / eV	Pred. (vac.)	1.358	1.298 (-0.060)	1.499 (+0.141)
	TD-DFT (vac.)	1.389	1.308 (-0.081)	1.501 (+0.112)
	TD-DFT (acetone)	1.395	1.334 (-0.061)	1.493 (+0.098)

The TD-DFT results of Table S3 agree well with the predictions for the 3Ac-Chl+ case (for both vacuum and acetone), showing minute changes for ΔE_{0-S1} compared to Chl *a*, and a small shift to lower ΔE_{0-T1}. For DVChl bf, TD-DFT ΔE_{0-S1} values are slightly lower than predicted, resulting in a downshift where the KRR would predict a rise in energy. ΔE_{0-S1} still remains close (less 0.06 eV different) to the Chl *a* excitation, which we consider close enough to possibly maintain original Chl *a* photophysics. Consequently, ΔE_{0-T1} of DVChl *bf* is also computed by TD-DFT to be lower in energy than the ML predictions. We assign this issue of vinyl-containing Chls to be generally red shifted to the vinyl group conformations, as discussed in the main article. Qualitatively, however, TD-DFT calculations agree with the KRR, also quantitatively in the case of 3Ac-Chl+. The solvent is found to be not relevant for the quality of the B band results.

S9: Comparison of ML data to conventional QC: DFT/MRCI

DFT/MRCI calculations for systems of the investigated size are challenging, since even high-end computers struggle with memory problems in several cases; unfortunately, we were thus unable to obtain any ΔE_{0-T1} values from DFT/MRCI with the available computing resources. For the other cases, fortunately, we found that gas phase vs. acetone results only differ by less than 0.01 eV, thus not warranting a separate "gas phase vs. acetone" discussion (cf. TD-DFT results), which simplifies the discussion greatly. We also restrict the discussion to the energies, as we were unable to obtain the f values consistently due to the computer memory issues mentioned above. Qualitatively we find that DFT/MRCI values agree with the predicted values, though the shifts resulting from DFT/MRCI are quantitatively closer to the TD-DFT results than to the predicted ones. The range of the differences between methods is however below 0.05 eV (Q band) or 0.1 eV (B band). This means that our predictions hold, showing a possible slight red shift for the predicted Q-shifted variants, although this could be dependent on the environment, as indicated by TD-DFT. For the B band, we are confident that the suggested Chl variants should be B band red shifted by about 0.15 eV compared to Chl *b*.

Table S4: Vertical DFT/MRCI excitation energy differences (in eV) to Chl f or Chl b for several predicted Chl variants, compared to ML-predicted and TD-DFT values (averaged from Table S1 and Table S2 gas phase/acetone calculations).

Method	$\Delta\Delta E_{0-S1}$(Target-Chl *f*) / eV		$\Delta\Delta E_{0-S3}$(Target-Chl b) / eV		
	Chl *df*	Chl *f+*	DVChl *b*	Chl *bb*	Chl *bd*
Pred. (vac.)	-0.02	-0.02	-0.16	-0.16	-0.09
TD-DFT (avg.)	+0.01	+0.05	-0.12	-0.14	-0.165
DFT/MRCI	-0.03	-0.02	-0.06	-0.12	-0.17

S10: Example QC inputs during the ML scheme

Input for PM6 pre-optimization (command line only)

```
#T OPT PM6 symmetry=none geom(nodistance,noangle,nodihedral)
symmetry=none
```

```
#IOp(2/9=1111, 2/11=2, 4/33=0) Guess(Always)
```

Input for DFT optimization (singlet and triplet) (command line only)

```
#T CAM-B3LYP/6-31G* OPT symmetry=none
geom(nodistance,noangle,nodihedral)
```

```
#iop(6/7=2, 4/33=0, 2/9=1111, 2/11=2) 5D 7F
```

Input for TD-DFT calculations (command line only)

```
#p CAM-B3LYP/6-31G* td(nstates=12, root=1) Symmetry=None GFINPUT
GFPRINT iop(6/7=3,9/40=5) 5D 7F
```

S11: Predicted values in Figures 3 and 5 of the main article

Table S5: Predicted excitation energies (E) and oscillator strengths (f) values of the explicitly considered Chl variants in the main article, for the excited states given in the first row. Energies include the shift for better comparison to the experimental maxima/values (Q states: -0.278 eV, B states: -0.615 eV, triplets: -0.019 eV).

	Q_y		Q_x		B_x		B_y		T_1
	E / eV	f	E / eV	f	E / eV	f	E / eV	f	E / eV
Chl *a*	2.144	0.255	2.522	0.037	3.466	0.881	3.724	0.698	1.357
Chl *b*	2.250	0.171	2.581	0.022	3.378	1.044	3.550	0.740	1.561
8OH-Chl	2.149	0.238	2.517	0.029	3.461	0.882	3.695	0.753	1.377
Chl *d*	2.087	0.239	2.447	0.033	3.410	0.945	3.689	0.718	1.287
Chl *f*	2.068	0.315	2.475	0.049	3.440	0.642	3.730	0.696	1.309
3Ac-Chl	2.144	0.230	2.498	0.028	3.447	0.969	3.706	0.670	1.359
DVChl *a*	2.157	0.230	2.536	0.026	3.424	1.063	3.694	0.790	1.381
DVChl *b*	2.237	0.148	2.588	-0.004	3.218	1.234	3.419	0.619	1.536
Chl *df*	2.047	0.324	2.326	0.080	3.390	0.553	3.689	0.519	1.220
Chl *f+*	2.046	0.359	2.338	0.105	3.359	0.361	3.658	0.572	1.230
Chl *bb*	2.312	0.082	2.637	0.028	3.222	1.093	3.292	0.601	1.679
Chl *bd*	2.186	0.175	2.488	0.018	3.288	1.073	3.510	0.716	1.457
3Ac-Chl+	2.151	0.290	2.413	0.096	3.396	0.528	3.679	0.641	1.298
DVChl *bf*	2.153	0.214	2.501	0.011	3.187	1.058	3.407	0.618	1.499